Title

In silico prediction of drug therapy in catecholaminergic polymorphic ventricular tachycardia.

Journal

The Journal of physiology, 594(3)

ISSN

0022-3751

Authors

Yang, Pei-Chi
Moreno, Jonathan D
Miyake, Christina Y
et al.

Publication Date

2016-02-01

DOI

10.1113/jp271282

Peer reviewed

J Physiol 594.3 (2016) pp 567–593

The Journal of Physiology

In silico prediction of drug therapy in catecholaminergic polymorphic ventricular tachycardia

Pei-Chi Yang[1], Jonathan D. Moreno[2], Christina Y. Miyake[3], Steven B. Vaughn-Behrens[1], Mao-Tsuen Jeng[1], Eleonora Grandi[1], Xander H. T. Wehrens[3,4], Sergei Y. Noskov[5] and Colleen E. Clancy[1]

[1] *Department of Pharmacology, School of Medicine, University of California, Davis, CA, USA*
[2] *Division of Cardiology, Department of Medicine, Barnes-Jewish Hospital, Washington University in St Louis, St Louis, MO, USA*
[3] *Cardiovascular Research Institute, Department of Molecular Physiology & Biophysics, Department of Medicine, Cardiology, Baylor College of Medicine, Houston, TX, USA*
[4] *Department of Pediatrics, Texas Children's Hospital, Baylor College of Medicine, and the Cardiovascular Research Institute, Houston, TX, USA*
[5] *Centre for Molecular Simulation, Department of Biological Sciences, Faculty of Science, University of Calgary, Calgary, Alberta, Canada*

Key points

- The mechanism of therapeutic efficacy of flecainide for catecholaminergic polymorphic ventricular tachycardia (CPVT) is unclear.
- Model predictions suggest that Na^+ channel effects are insufficient to explain flecainide efficacy in CPVT.
- This study represents a first step toward predicting therapeutic mechanisms of drug efficacy in the setting of CPVT and then using these mechanisms to guide modelling and simulation to predict alternative drug therapies.

Abstract Catecholaminergic polymorphic ventricular tachycardia (CPVT) is an inherited arrhythmia syndrome characterized by fatal ventricular arrhythmias in structurally normal hearts during β-adrenergic stimulation. Current treatment strategies include β-blockade, flecainide and ICD implementation – none of which is fully effective and each comes with associated risk. Recently, flecainide has gained considerable interest in CPVT treatment, but its mechanism of action for therapeutic efficacy is unclear. In this study, we performed *in silico* mutagenesis to construct a CPVT model and then used a computational modelling and simulation approach to make predictions of drug mechanisms and efficacy in the setting of CPVT. Experiments were carried out to validate model results. Our simulations revealed that Na^+ channel effects are insufficient to explain flecainide efficacy in CPVT. The pure Na^+ channel blocker lidocaine and the antianginal ranolazine were additionally tested and also found to be ineffective. When we tested *lower dose* combination therapy with flecainide, β-blockade and CaMKII inhibition, our model predicted superior therapeutic efficacy than with flecainide monotherapy. Simulations indicate a polytherapeutic approach may mitigate side-effects and proarrhythmic potential plaguing CPVT pharmacological management today. Importantly, our prediction of a novel polytherapy for CPVT was confirmed experimentally. Our simulations suggest that flecainide therapeutic efficacy in CPVT is unlikely to derive from primary interactions with the Na^+ channel, and benefit may be gained from an alternative multi-drug regimen.

P.-C. Yang and J. D. Moreno contributed equally.

DOI: 10.1113/JP271282

(Resubmitted 15 July 2015; accepted after revision 22 October 2015; first published online 30 October 2015)
Corresponding author C. E. Clancy: Department of Pharmacology, School of Medicine, University of California, Davis, Genome Building Rm 3503, Davis, CA 95616-8636, USA. Email: ceclancy@ucdavis.edu

Abbreviations APD, action potential duration; BCL, Basic Cycle Length; CaMKII, Ca^{2+}/calmodulin-dependent protein kinase; CASQ2, calsequestrin; CPVT, catecholaminergic polymorphic ventricular tachycardia; DAD, delayed afterdepolarizations; EAD, early afterdepolarizations; ICD, implantable cardioverter defibrillator; ISO, isoproterenol; KO, knockout; PKA, cAMP-dependent protein kinase; PMF, potential of mean force; P_o, open probability; RyR2, ryanodine receptor; SCaR, spontaneous Ca^{2+} release event; T_c, mean closed time; T_o, mean open time; TB, tonic block; VT, ventricular tachycardia; WT, wild-type.

Introduction

First-line pharmacotherapy for treating catecholaminergic polymorphic ventricular tachycardia (CPVT) patients utilizes β-blockade at maximally tolerated doses; however, 30% of patients continue to experience arrhythmic episodes and often require mechanical implantable cardioverter defibrillator (ICD) implantation (Liu *et al.* 2008). β-Blockade is associated with fatigue, diminished physical activity level and reduced quality of life, while ICD discharge is associated with significant pain and anxiety, which can induce additional episodes of electrical storm (Sears *et al.* 1999; Nakamura *et al.* 2007).

CPVT is an inherited arrhythmia syndrome arising from mutations in the ryanodine receptor (RyR2) as well as the calcium buffer and regulator of RyR2, calsequestrin (CASQ2). As its name suggests, CPVT sets up a pathological substrate for arrhythmogenesis under the influence of a catecholamine surge, which leads to bidirectional and polymorphic ventricular tachycardia. Sudden cardiac arrest and death are not uncommon for individuals harbouring CPVT mutations, and a lethal episode may present as the first manifestation of disease (Priori *et al.* 2002).

Flecainide, a class IC antiarrhythmic suppresses the emergence of CPVT in both mice harbouring the CASQ2(−/−) mutation and humans with either a CASQ2 or RYR2 (S412G) mutation (Watanabe *et al.* 2009; van der Werf *et al.* 2011). However, the mechanism and efficacy of flecainide remain disputed. For example, Katz *et al.* (2010) found little efficacy for CASQ2 subtypes, while Liu *et al.* suggested virtually no effect on Ca^{2+} handling properties, rather proposing that flecainide is effective due to its Na^+ channel blocking properties (Watanabe *et al.* 2011; Liu *et al.* 2011*a*). Still other studies demonstrated flecainide interaction and blockade of RyR2 (Hilliard *et al.* 2010; Galimberti & Knollmann, 2011; Mehra *et al.* 2014).

Studies of other class I antiarrhythmics showed that only those that modulated RyR2 activity demonstrated efficacy in models of CPVT, including propafenone (Hwang *et al.* 2011). Moreover, the type of interaction with the RyR2 was found to be significant as well; tetracaine, an RyR2 closed state blocker, failed to regulate Ca^{2+} properties in a CASQ2(−/−) model of CPVT (Galimberti & Knollmann, 2011). The late Na^+ channel blocker ranolazine has also been studied for treatment of CPVT; however, two studies reveal conflicting results: Parikh *et al.* (2012) demonstrated strong interaction between ranolazine and RyR2, whereas Galimberti & Knollmann (2011) failed to demonstrate such an interaction.

Discrepant experimental observations, likely to be due to different experimental set-ups and models of CPVT, make reconciling the aforementioned studies difficult. Thus, the focus of the present study is to use a computational modelling approach to understand the dominant mechanism(s) underlying antiarrhythmic drug success and failure. In particular, is the effect of flecainide to normalize aberrant Na^+ channel activation sufficient to explain observed clinical efficacy? The latter would be particularly important, given the wealth of clinical (The Cardiac Arrhythmia Suppression Trial (CAST) Investigators, 1989; Nakamura *et al.* 2007) and experimental data (Moreno *et al.* 2011) that reveal flecainide-induced proarrhythmia. Finally, can we use the model as a therapeutic prediction tool to optimize a multidrug regimen in CPVT?

Methods

Ethics approval

Animal use was approved by the Institutional Animal Care and Use Committee, Baylor College of Medicine, and conformed to the *Guide for the Care and Use of Laboratory Animals* (National Research Council, 2011).

Experimental methods

Eight animals (six R176Q/+ and two wild-type (WT)) were studied with ECG telemetry as previously described (van Oort *et al.* 2010). Telemeters (Data Sciences International, St Paul, MN, USA) were implanted in the abdominal cavity with subcutaneous lead placement in a lead II configuration. Following telemetry implantation, mice were injected with subcutaneous 0.3 mg kg^{-1} buprenorphine. The isoflurane was discontinued and mice were placed on a warming pad with blow-by oxygen. They were observed continuously until awake with normal breathing pattern and spontaneous movement. The mice were observed continuously for the first 2 h

then daily for 7 days. Buprenophine, 0.2–0.3 mg kg^{-1} subcutaneous injection, was provided every 6–12 h for the first 24 h. Ambulatory telemetry recordings were obtained after all animals had at least 7 days' recovery from surgery and a 24 h baseline recording. Repeat baseline recordings were obtained 15 min prior to all injections. Mice were injected with a single intraperitoneal (i.p.) dose of adrenaline (120 mg kg^{-1}, Sigma-Aldrich, St Louise, MO, USA) and caffeine (120 mg kg^{-1}, Avantor Performance Materials, Center Valley, PA, USA) in sterile saline followed by continuous 24 h telemetry recordings. After a 7 day wash-out period, all mice underwent repeated injections with pretreatment. Baseline ECG telemetry was recorded for 15 min. Separate i.p. injections were given of flecainide (12 mg kg^{-1}, Sigma-Aldrich), metoprolol (10 mg kg^{-1}, Sigma-Aldrich) and KN-93 (30 μmol kg^{-1}, Calbiochem). All drugs were mixed in sterile water. After 30 min, mice were injected with a single i.p. dose of adrenaline (2 mg kg^{-1}) and caffeine (120 mg kg^{-1}). Following injection of adrenaline and caffeine, the mice were monitored by telemetry for a total of 8 h. Data collection was performed using Dataquest A.R.T. version 4.31 (Data Sciences International, St Paul, MN, USA). Off-line analysis was performed by ECG Auto analysis version 3.1 (EMKA technologies, Falls Church, VA, USA).

Molecular dynamics and free energy simulations

Force-field parameters for flecainide were developed using the general automated atomic model parameterization (GAAMP) server developed by Huang & Roux (2013). Briefly, all geometry optimization, charge fitting and torsional parameter fitting were done using B3LYP functional at the 6–31G*(2d,2p) level of theory. Umbrella sampling simulations for partitioning of the neutral and cationic forms of flecainide into model POPE bilayer (128 lipids) were performed using a protocol described previously by Li *et al.* (2008). Harmonic constraints of 5 kcal $(\text{mol Å}^2)^{-1}$ were applied to the drug's centre of mass along the reaction coordinate spanning 62 Å from −31 Å to 31 Å normal to the membrane plane. We used five starting conformations for the drug and 124 windows spaced every 0.5 Å to describe drug partitioning into the bilayer. A flat-bottomed cylindrical restraint with $R = 15$ Å was used to confine drug in the xy plane along the reaction coordinate. It allows for good sampling in a lateral plane. Each potential of mean force (PMF) window was equilibrated for 2.5 ns in the presence of restraining potential and then subjected to a 5 ns production run. The resulting 1D PMF was reconstructed with the weighted histogram analysis method (WHAM) (Roux, 1995). The WHAM convergence tolerance was set at 0.0001 kcal mol^{-1}. We used symmetrized density to compute resulting PMFs. The statistical uncertainties were estimated by separating the data into seven blocks and were found to be within ±1.5 kcal mol^{-1} for neutral and charged forms of flecainide, respectively.

Computational ventricular myocyte models

Briefly, we developed mouse and rabbit *in silico* models of catecholaminergic polymorphic ventricular tachycardia (CPVT) by 'knocking out' the SR Ca^{2+} buffer calsequestrin (Kornyeyev *et al.* 2012) in the Morotti–Grandi mouse cardiac cell model (Morotti *et al.* 2014) and in the Soltis–Saucerman rabbit cardiac cell model (Soltis & Saucerman, 2010), respectively. Flecainide interactions with the ryanodine receptor were modelled assuming open state associations (Hilliard *et al.* 2010). We also incorporated the model of the cardiac Na^+ channel and I_{Kr} and their interaction with flecainide as previously (Moreno *et al.* 2011, 2013). We utilized the Morotti–Grandi computational model for mouse (Morotti *et al.* 2014) and the Soltis–Saucerman computational model for rabbit (Soltis & Saucerman, 2010), which included all the relevant components required for a detailed analysis, including accurate cellular electrophysiology, Ca^{2+} handling (Shannon *et al.* 2004) and the cAMP-dependent protein kinase (PKA) (Saucerman *et al.* 2003) and Ca^{2+}/calmodulin-dependent protein kinase (CaMKII) (Soltis & Saucerman, 2010) phosphorylation pathways. The computational model for flecainide interaction with the cardiac Na^+ channel is from (Moreno *et al.* 2011), with adaptations designed to recreate the CPVT phenotype and flecainide's interaction with the RyR2, informed and validated by experimental data (Hilliard *et al.* 2010; Hwang *et al.* 2011).

Wild-type Na^+ channel models and inclusion of drug binding

The wild-type drug-free Na^+ channel model was used as previously described (Moreno *et al.* 2013). The Na^+ drug-channel model parameters for the on- and off-rates of flecainide, ranolazine and lidocaine are taken from experiments where available. These include diffusion rates that indicate drug on-rates 'k_{on}' = [drug] × D (diffusion rate) and affinities (K_d) to discrete conformations that determine drug off-rates 'k_{off}' = K_d × D (diffusion rate). Rates were also constrained by experimental data (described in detail below) and microscopic reversibility as in Colquhoun *et al.* (2004). The transition rates are given in Table 1.

Flecainide. The flecainide model was used as previously described (Moreno *et al.* 2011), but now includes a drug-bound bursting regime (drug binding to red states as indicated in Scheme 1; Tope 8 states are 'normal' gating mode, while red states indicate burst mode). Rate constants in the upper (normal mode) states are from

Table 1. Markov model transition rates (ms^{-1}) for Drug free WT Na^+ channel

States of Markov model	*Rate constants*
IC3 →IC2, C3→C2, BC3→BC2	$\alpha 11 = 8.5539/(7.4392e\text{-}2^{*}\exp(-V/17.0)+2.0373e\text{-}1^{*}\exp(-V/150))$
IC2→IF, C2→C1, BC2→BC1	$\alpha 12 = 8.5539/(7.4392e\text{-}2^{*}\exp(-V/15.0)+2.0373e\text{-}1^{*}\exp(-V/150))$
C1→O, BC1→BO	$\alpha 13 = 8.5539/(7.4392e\text{-}2^{*}\exp(-V/12.0)+2.0373e\text{-}1^{*}\exp(-V/150))$
IC2→IC3, C2→C3, BC2→BC3	$\beta 11 = 7.5215e\text{-}2^{*}\exp(-V/20.3)$
IF→IC2, C1→C2, BC1→BC2	$\beta 12 = 2.7574^{*}\exp(-(V-5)/20.3)$
O→C1, BO→BC1	$\beta 13 = 4.7755e\text{-}1^{*}\exp(-(V-10)/20.3)$
IC3→C3, IC2→C2, IF→C1	$\alpha 3 = 5.1458e\text{-}6^{*}\exp(-V/8.2471)$
C3→IC3, C2→IC2, C1→IF	$\beta 3 = 6.1205^{*}\exp(V/13.542)$
O→IF	$\alpha 2 = 13.370^{*}\exp(V/43.749)$
IF→O	$\beta 2 = (\alpha 13^{*}\ \alpha 2^{*}\ \alpha 3)/(\beta 13^{*}\ \beta 3)$
O→IS	$\alpha x = 3.4229e\text{-}2^{*}\alpha 2$
IS→O	$\beta x = 1.7898e\text{-}2^{*}\alpha 3$
C3, C2, C1, O → BC3, BC2, BC1, BO	$\mu 1 = 2.0462e\text{-}7$
BC3, BC2, BC1, BO → C3, C2, C1,O	$\mu 2 = 8.9731e\text{-}4$

Scheme 1

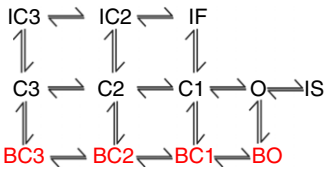

Moreno *et al.* (2011). Bursting state affinity for the charged form of flecainide was initially set at the value found by assuming the affinity of tonic block of late I_{Na} was equal to K_d at −100 mV. The value for $K_{d,0}$ was then calculated and used as an initial value in the optimization. For example, the affinity of tonic block (TB) $I_{Na,L}$ for WT is ∼44 μM (Nagatomo *et al.* 2000); if that value is assumed to equal $K_{d,-100mV}$, $K_{d,0,bursting}$ was initially set at 3.202 μM (e.g. the $K_{d,0,bursting}$ that would give $K_{d,-100mV,bursting} = 44\ \mu$M). The optimized $K_{d,0,bursting}$ was 95.2165 μM. Full parameters are given in Table 2.

Ranolazine. The ranolazine–Na^+ channel drug interaction model was as previously described (Moreno *et al.* 2013) and the transition rates are given in Table 3.

Lidocaine. The wild-type lidocaine model was as previously described (Moreno *et al.* 2011), but now includes a drug-bound bursting (lower 4 states) regime. Non-bursting rates were from (Moreno *et al.* 2011). Bursting state affinity for the charged form of lidocaine was initially set at the value found by assuming the affinity of tonic block of late I_{Na} was equal to K_d at −100 mV. $K_{d,0}$ was then calculated and used as an initial value in the optimization. For example, the affinity of TB $I_{Na,L}$ for WT is ∼12 μM (Fedida *et al.* 2006); if that value is assumed to equal $K_{d,-100mV}$, $K_{d,0,bursting}$ was initially set at 0.80 μM (e.g. the $K_{d,0,bursting}$ that would give $K_{d,-100mV,bursting} = 12\ \mu$M). The optimized $K_{d,0,bursting}$ was 0.9810 μM. The transition rates are given in Table 4.

RyR2–flecainide drug-channel interaction model development

The Shannon–Bers Markov model formulation of the RyR2 (Shannon *et al.* 2004) was modified to include a drug bound state DO with transitions $k_{on} = D \times [\text{drug}]$ and $k_{off} = D \times IC_{50,drug}$ to and from the open state O, which represent the drug diffusing to the receptor and binding or dissociating from the channel, respectively, as done previously (Moreno *et al.* 2011). The diffusion rate of flecainide (Scheme 2) was estimated at 5500 M^{-1} ms^{-1} (Zhu *et al.* 2006).

Scheme 2

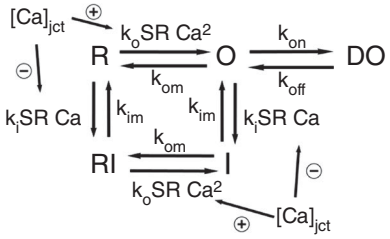

Isoproterenol-stimulated Ca^{2+} waves in CASQ2 knockout (KO) CASQ2(−/−) mice were inhibited by flecainide with an IC_{50} of 2.0 ± 0.2 μM (Hwang *et al.* 2011), while other experimental preparations measured an IC_{50} range from 2 to 17 μM (Brunton *et al.* 2010; Hilliard *et al.* 2010; Hwang *et al.* 2011; Mehra *et al.* 2014). Drug binding was modelled as open-state block, using experimental data for drug affinity to the open state to determine off and on rates, respectively. We also predicted cases for variable flecainide $IC_{50} = 3$, 4, and 5 μM shown in Fig. 1. We examined the cases of 3, 4 and 5 μM of IC_{50} acting on each of the targets under the influence of 1 μM isoproterenol, over a range of clinically relevant pacing frequencies, from 0.5 to 3.0 Hz (30–180 beat min^{-1}; Leenhardt *et al.* 1995), at 0.01 Hz increments.

We assumed rapid partitioning of flecainide into its charged (98% at pH 7.4, $pK_a = 9.3$) and neutral (2%)

Table 2. Markov model transition rates (ms^{-1}) for Flecainide

Parameter Name	*Value*
$k_{on} = k_{closed,\ on}$	[D+]*Diffusion
$k_{off} = k_{closed,\ off}$	$k_{d,\ open}$ *Diffusion; ($kd_{open} = 11.2e\text{-}6*\exp(-0.7*V*F/R*T)$)
$k_{bursting,\ on} = k_{closed\ bursting,\ on}$	[D+]*Diffusion
$k_{bursting,\ off} = k_{closed\ bursting,\ off}$	$kd_{Bursting,Open}$ *Diffusion; ($kd_{Bursting,Open} = 95.2165e\text{-}6*\exp(-0.7*V*F/R*T)$)
$k_{neutral,\ on}$	[D]*Diffusion
$k_{neutral,\ off}$	400e-6*Diffusion
$k_{neutral,\ inactivated,\ on}$	$k_{neutral,\ on}/2$
$k_{neutral,\ inactivated,\ off}$	5.4e-6*Diffusion
$k_{neutral,\ closed,\ on}$	$k_{neutral,\ on}/2$
$k_{neutral,\ closed,\ off}$	800e-6*Diffusion
Diffusion	5500 $M^{-1}ms^{-1}$
States of Markov model	***Rate constants***
$D^+IC3 \rightarrow D^+IC2$, $D^+C3 \rightarrow D^+C2$, DIC3 →DIC2, DC3→DC2	$\alpha 11$
$D^+IC2 \rightarrow D^+IF$, $D^+C2 \rightarrow D^+C1$, DIC2→DIF, DC2→DC1	$\alpha 12$
$D^+IC2 \rightarrow D^+IC3$, $D^+C2 \rightarrow D^+C3$, DIC2→DIC3, DC2→DC3	$\beta 11$
$D^+IF \rightarrow D^+IC2$, $D^+C1 \rightarrow D^+C2$, DIF→DIC2, DC1→DC2	$\beta 12$
$D^+O \rightarrow D^+IS$	$\alpha x1 = 5.7839e\text{-}5*\alpha x$
$D^+IS \rightarrow D^+O$	$\beta x1 = 1.6689e\text{-}8*\beta x$
DO→DIS	$\alpha x2 = 2.6126e\text{-}1*\alpha x$
$D^+C1 \rightarrow D^+O$	$\alpha 13c = 3.6324e\text{-}3*\alpha 13$
DC1→DO	$\alpha 13n = 2.6452e{+}0*\alpha 13$
$D^+O \rightarrow D^+C1$	$\beta 13c = (\beta 13*kcon*koff*\alpha 13c)/(kon*kcoff*\alpha 13)$
DO→DC1	$\beta 13n = (\beta 13*kc\_on*\alpha 13n*k\_off)/(kc\_off*\alpha 13*k\_on)$
DIS→DO	$\beta x2 = (\beta x*k\_on*\alpha x2*ki\_off)/(\alpha x*ki\_on*k\_off)$
$D^+O \rightarrow D^+IF$	$\alpha 22 = 1.4847e{+}3*\alpha 2$
DO→DIF	$\alpha\_22 = 4.2385e{+}1*\alpha 2$
$D^+IF \rightarrow D^+O$	$\beta 22 = (\alpha 13c*\alpha 22*\alpha 33)/(\beta 13c*\beta 33)$
DIF→DO	$\beta\_22 = (\alpha\_33*\alpha 13n*\alpha\_22)/(\beta\_33*\beta 13n)$
$D^+C3 \rightarrow D^+IC3$, $D^+C2 \rightarrow D^+IC2$, $D^+C1 \rightarrow D^+IF$	$\beta 33 = 1.7352e\text{-}6*\beta 3$
DC3→DIC3, DC2→DIC2, DC1→DIF	$\beta\_33 = 2.1181e{+}0*\beta 3$
$D^+IC3 \rightarrow D^+C3$, $D^+IC2 \rightarrow D^+C2$, $D^+IF \rightarrow D^+C1$	$\alpha 33 = 6.7505e\text{-}5*\alpha 3$
DIC3→DC3, DIC2→DC2, DIF→DC1	$\alpha\_33 = (ki\_off*\alpha 3*kc\_on*\beta\_33)/(ki\_on*kc\_off*\beta 3)$
$D^+IF \rightarrow D^+IT$	$\alpha 44 = 2.4135*\alpha 2$
$D^+IT \rightarrow D^+IF$	$\beta 44 = 4.9001e\text{-}2*\alpha 3$
DIF→DIT	$\alpha\_44 = 1.0326e\text{-}3*\alpha 2$
DIT→DIF	$\beta\_44 = 2.1378e\text{-}2*\alpha 3$

fractions (Liu *et al.* 2003), diffusion of the neutral component across the membrane, and equilibration on the cytosolic side, resulting in equimolar concentrations of flecainide inside and outside of the cell, consistent with experimental observations and the mechanism of flecainide's interaction with the Na^+ channel (Liu *et al.* 2003). The kinetics of the state transitions for the channel are adjusted for temperature by a Q_{10} factor of 1.5 (Sitsapesan *et al.* 1991). The presence of a 20% RyR sub-conductance state in response to flecainide binding of the channel (Hilliard *et al.* 2010) is modelled at the whole cell level as a reduction to 20% maximal conductance of the channel.

In single channel simulations mimicking the experimental conditions tested, the IC_{50} of 16 μM was used to validate the model. It is important, however, to justify the use of the 2 μM IC_{50} value used in cellular and tissue level simulations. The 16 μM IC_{50} value corresponds to single channel conditions (Hilliard *et al.* 2010), which does not account for the influence of coupling between adjacent ryanodine receptors on the kinetics of the channel (Marx *et al.* 2001). Similarly, the IC_{50} value of 16 μM

Table 3. Markov model transition rates (ms^{-1}) for Ranolazine

Parameter Name	*Value*
$k_{on} = k_{closed,\ on}$	[D+]*Diffusion
$k_{off} = k_{closed,\ off}$	$k_{d,\ open}$ *Diffusion; (kd_{open} = 100.5e-6*exp(-0.7*V*F/R*T))
$k_{bursting,\ on} = k_{closed\ bursting,\ on}$	[D+]*Diffusion
$k_{bursting,\ off} = k_{closed\ bursting,\ off}$	$kd_{Bursting,Open}$ *Diffusion; ($kd_{Bursting,Open}$ = 1.5012e-6*exp(-0.7*V*F/R*T))
$k_{neutral,\ on}$	[D]*Diffusion
$k_{neutral,\ off}$	400e-6*Diffusion
$k_{neutral,\ inactivated,\ on}$	$k_{neutral,\ on}$
$k_{neutral,\ inactivated,\ off}$	5.4e-6*Diffusion
$k_{neutral,\ closed,\ on}$	$k_{neutral,\ on}$
$k_{neutral,\ closed,\ off}$	800e-6*Diffusion
Diffusion	5500 $M^{-1}ms^{-1}$
States of Markov model	***Rate constants***
$D^+IC3 \rightarrow D^+IC2$, $D^+C3 \rightarrow D^+C2$, $DIC3 \rightarrow DIC2$, $DC3 \rightarrow DC2$	$\alpha 11$
$D^+IC2 \rightarrow D^+IF$, $D^+C2 \rightarrow D^+C1$, $DIC2 \rightarrow DIF$, $DC2 \rightarrow DC1$	$\alpha 12$
$D^+IC2 \rightarrow D^+IC3$, $D^+C2 \rightarrow D^+C3$, $DIC2 \rightarrow DIC3$, $DC2 \rightarrow DC3$	$\beta 11$
$D^+IF \rightarrow D^+IC2$, $D^+C1 \rightarrow D^+C2$, $DIF \rightarrow DIC2$, $DC1 \rightarrow DC2$	$\beta 12$
$D^+O \rightarrow D^+IS$	$\alpha x1 = 4.4923e{+}3 * \alpha x$
$D^+IS \rightarrow D^+O$	$\beta x1 = 2.7031e\text{-}1 * \beta x$
$DO \rightarrow DIS$	$\alpha x2 = 1.4947e{+}1 * \alpha x$
$D^+C1 \rightarrow D^+O$	$\alpha 13c = 3.6811 * \alpha 13$
$DC1 \rightarrow DO$	$\alpha 13n = 2.3570e{+}2 * \alpha 13$
$D^+O \rightarrow D^+C1$	$\beta 13c = (\beta 13 * kcon * koff * \alpha 13c)/(kon * kcoff * \alpha 13)$
$DO \rightarrow DC1$	$\beta 13n = (\beta 13 * kc\_on * \alpha 13n * k\_off)/(kc\_off * \alpha 13 * k\_on)$
$DIS \rightarrow DO$	$\beta x2 = (\beta x * k\_on * \alpha x2 * ki\_off)/(\alpha x * ki\_on * k\_off)$
$D^+O \rightarrow D^+IF$	$\alpha 22 = 6.8705e{+}4 * \alpha 2$
$DO \rightarrow DIF$	$\alpha\_22 = 2.1182e{+}2 * \alpha 2$
$D^+IF \rightarrow D^+O$	$\beta 22 = (\alpha 13c * \alpha 22 * \alpha 33)/(\beta 13c * \beta 33)$
$DIF \rightarrow DO$	$\beta\_22 = (\alpha\_33 * \alpha 13n * \alpha\_22)/(\beta\_33 * \beta 13n)$
$D^+C3 \rightarrow D^+IC3$, $D^+C2 \rightarrow D^+IC2$, $D^+C1 \rightarrow D^+IF$	$\beta 33 = 1.7561e\text{-}1 * \beta 3$
$DC3 \rightarrow DIC3$, $DC2 \rightarrow DIC2$, $DC1 \rightarrow DIF$	$\beta\_33 = 1.2197e\text{-}3 * \beta 3$
$D^+IC3 \rightarrow D^+C3$, $D^+IC2 \rightarrow D^+C2$, $D^+IF \rightarrow D^+C1$	$\alpha 33 = 4.0832e\text{-}2 * \alpha 3$
$DIC3 \rightarrow DC3$, $DIC2 \rightarrow DC2$, $DIF \rightarrow DC1$	$\alpha\_33 = (ki\_off * \alpha 3 * kc\_on * \beta\_33)/(ki\_on * kc\_off * \beta 3)$

for spark inhibition in permeabilized myocytes cannot be used, due to the constant maintenance of $[Ca^{2+}]$ in those experiments – the high concentration of Ca^{2+} used to elicit consistent Ca^{2+} sparks in experiments is static and is an unrealistic representation of paced myocytes (Galimberti & Knollmann, 2011). The high external Ca^{2+} concentration used would cause a higher IC_{50} than that seen using a lower Ca^{2+} concentration in the intact myocyte used to generate Ca^{2+} waves during diastole, due to a persistently overactive ryanodine receptor by constitutive cytosolic activation.

Thus the measured IC_{50} for wave inhibition in the isoproterenol-stimulated Ca^{2+} waves in CASQ2(−/−) mice ($IC_{50} = 2.0 \pm 0.2\ \mu M$; Hwang *et al.* 2011), was used, since it reflects realistic conditions for our model system. Its weakness is that the IC_{50} does not separate out external contributions to the IC_{50}, such as lowered junctional Ca^{2+} by I_{NCX} activity via lowered $[Na^+]$. Experiments in paced rat myocytes indicate that this contribution may significantly influence flecainide's ability to inhibit spontaneous Ca^{2+} wave formation, and thus future work will need to evaluate whether the contribution of I_{NCX} regulation of Na^+ is indeed significant in influencing flecainide's efficacy (Sikkel *et al.* 2013).

$$k_{CaSR} = Max_{SR} - \frac{Max_{SR} - Min_{SR}}{1 + \left(\frac{EC_{50,SR}}{[Ca]_{SR}}\right)^{H}_{SR}}$$

Table 4. Markov model transition rates (ms^{-1}) for Lidocaine

Parameter Name	*Value*
kon = kclosed, on	[D+]*Diffusion
$k_{off} = k_{closed,\ off}$	$k_{d,\ open}$ *Diffusion; (kd_{open} = 318e-6*exp(-0.7*V*F/R*T))
$k_{bursting,\ on} = k_{closed\ bursting,\ on}$	[D+]*Diffusion
$k_{bursting,\ off} = k_{closed\ bursting,\ off}$	$kd_{Bursting,Open}$ *Diffusion; ($kd_{Bursting,Open}$ = 0.981e-6*exp(-0.7*V*F/R*T))
$k_{neutral,\ on}$	[D]*Diffusion
$k_{neutral,\ off}$	400e-6*Diffusion
$k_{neutral,\ inactivated,\ on}$	$k_{neutral,\ on}$/2
$k_{neutral,\ inactivated,\ off}$	3.4e-6*Diffusion
$k_{neutral,\ closed,\ on}$	$k_{neutral,\ on}$/2
$k_{neutral,\ closed,\ off}$	900e-6*Diffusion
Diffusion	500 $M^{-1}ms^{-1}$
States of Markov model	***Parameters***
$D^+IC3 \rightarrow D^+IC2$, $D^+C3 \rightarrow D^+C2$, $DIC3 \rightarrow DIC2$, $DC3 \rightarrow DC2$	$\alpha 11$
$D^+IC2 \rightarrow D^+IF$, $D^+C2 \rightarrow D^+C1$, $DIC2 \rightarrow DIF$, $DC2 \rightarrow DC1$	$\alpha 12$
$D^+IC2 \rightarrow D^+IC3$, $D^+C2 \rightarrow D^+C3$, $DIC2 \rightarrow DIC3$, $DC2 \rightarrow DC3$	$\beta 11$
$D^+IF \rightarrow D^+IC2$, $D^+C1 \rightarrow D^+C2$, $DIF \rightarrow DIC2$, $DC1 \rightarrow DC2$	$\beta 12$
$D^+O \rightarrow D^+IS$	$\alpha x1 = 6.3992e\text{-}7*\alpha x$
$D^+IS \rightarrow D^+O$	$\beta x1 = 1.3511e{+}0*\beta x$
$DO \rightarrow DIS$	$\alpha x2 = 1.3110e\text{-}1*\alpha x$
$D^+C1 \rightarrow D^+O$	$\alpha 13c = 5.6974e\text{-}3*\alpha 13$
$DC1 \rightarrow DO$	$\alpha 13n = 8.4559e{+}1*\alpha 13$
$D^+O \rightarrow D^+C1$	$\beta 13c = (\beta 13*kcon*koff*\alpha 13c)/(kon*kcoff*\alpha 13)$
$DO \rightarrow DC1$	$\beta 13n = (\beta 13*kc\_on*\alpha 13n*k\_off)/(kc\_off*\alpha 13*k\_on)$
$DIS \rightarrow DO$	$\beta x2 = (\beta x*k\_on*\alpha x2*ki\_off)/(\alpha x*ki\_on*k\_off)$
$D^+O \rightarrow D^+IF$	$\alpha 22 = 6.7067e\text{-}6*\alpha 2$
$DO \rightarrow DIF$	$\alpha\_22 = 1.7084e\text{-}5*\alpha 2$
$D^+IF \rightarrow D^+O$	$\beta 22 = (\alpha 13c*\alpha 22*\alpha 33)/(\beta 13c*\beta 33)$
$DIF \rightarrow DO$	$\beta\_22 = (\alpha\_33*\alpha 13n*\alpha\_22)/(\beta\_33*\beta 13n)$
$D^+C3 \rightarrow D^+IC3$, $D^+C2 \rightarrow D^+IC2$, $D^+C1 \rightarrow D^+IF$	$\beta 33 = 1.9698e\text{-}5*\beta 3$
$DC3 \rightarrow DIC3$, $DC2 \rightarrow DIC2$, $DC1 \rightarrow DIF$	$\beta\_33 = 4.8477e{+}0*\beta 3$
$D^+IC3 \rightarrow D^+C3$, $D^+IC2 \rightarrow D^+C2$, $D^+IF \rightarrow D^+C1$	$\alpha 33 = 3.2976e{+}0*\alpha 3$
$DIC3 \rightarrow DC3$, $DIC2 \rightarrow DC2$, $DIF \rightarrow DC1$	$\alpha\_33 = (ki\_off*\alpha 3*kc\_on*\beta\_33)/(ki\_on*kc\_off*\beta 3)$

$$k_{oSRCa} = \frac{k_{oCa}}{k_{CaSR}}$$

$$k_{iSRCa} = k_{iCa} k_{CaSR}$$

$$\frac{dR}{dt} = \left(k_{im}RI - k_{iSRCa}[Ca]_{jct}R\right) - \left(k_{oSRCa}\,[Ca]_{jct}^2\,R - k_{om}O\right)$$

$$\frac{dO}{dt} = \left(k_{oSRCa}\,[Ca]_{jct}^2\,R - k_{om}O\right) - \left(k_{iSRCa}[Ca]_{jct}O - k_{im}I\right) - (k_{on}O - k_{off}DO)$$

$$\frac{dI}{dt} = \left(k_{iSRCa}[Ca]_{jct}O - k_{im}I\right) - \left(k_{om}I - k_{oSRCa}\,[Ca]_{jct}^2\,RI\right)$$

$$\frac{dDO}{dt} = k_{on}O - k_{off}DO$$

$$RI = \left(k_{om}I - k_{oSRCa}[Ca]_{jct}^2 RI\right) - \left(k_{im}RI - k_{iSRCa}[Ca]_{jct}R\right)$$

$$J_{SRCaRel} = k_s\,(O + 0.2 \times DO) \times \left([Ca]_{SR} - [Ca]_{jct}\right)$$

$$J_{SRLeak} = K_{SRleak}\left([Ca]_{SR} - [Ca]_{jct}\right)$$

The parameters are presented in Table 5.

Simulation of I_{Kr} blockade

To simulate the effects of flecainide or ranolazine on I_{Kr} current, we decreased the peak conductance, G_{IKr} in a concentration dependent fashion using a

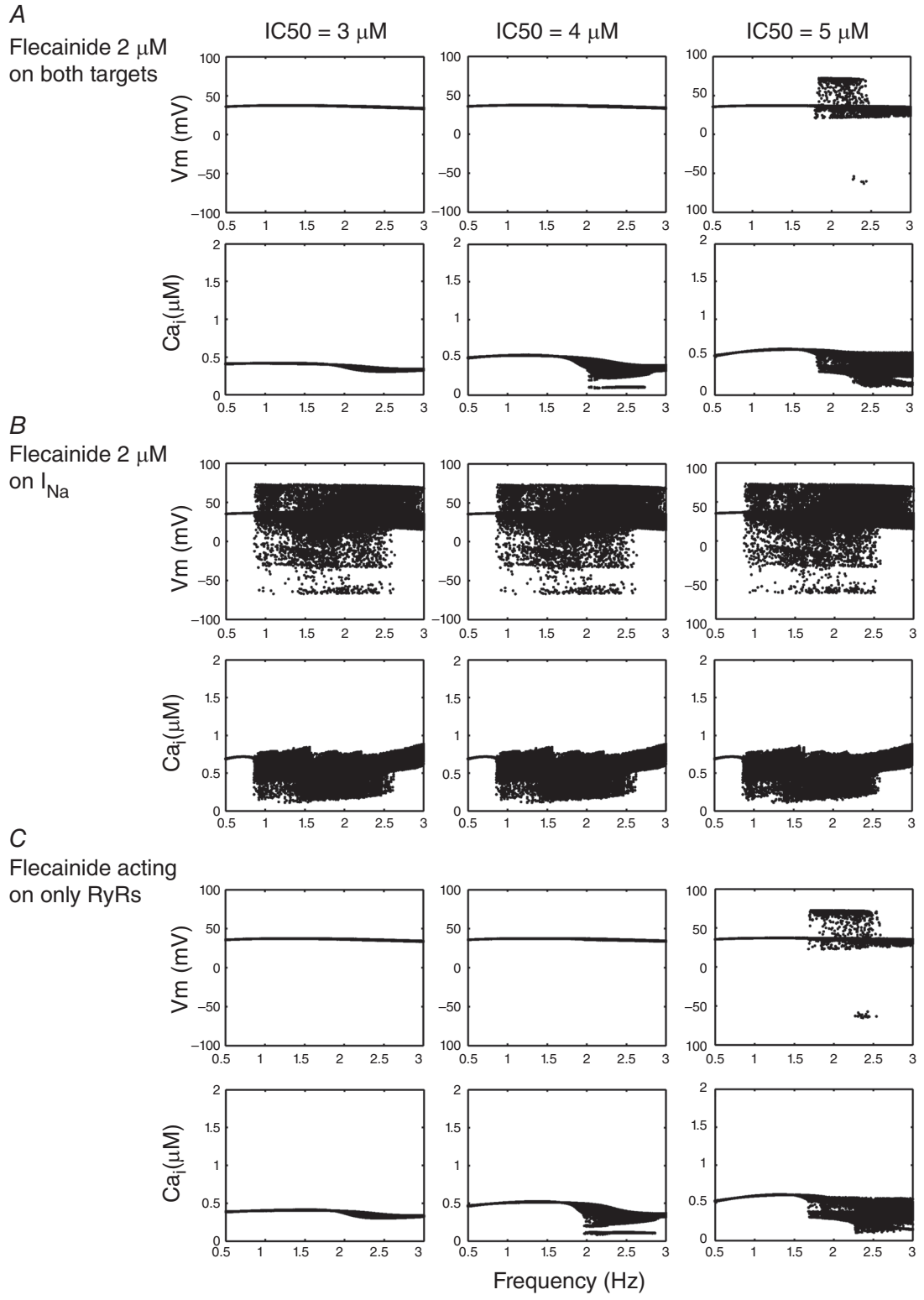

Figure 1. Testing IC_{50} of flecainide in the cell model for I_{Na}, RyR2 and both targets in combination
Voltage dynamics is shown for each IC_{50} case, and the voltage and Ca^{2+} transient maxima are binned for each pacing frequency between 0.5 and 3 Hz during the second half of a 2 min simulation time course. *A*, CASQ2(−/−) myocytes with 3, 4 and 5 μM IC_{50} effects on both Na^+ channels and RyRs. *B*, flecainide interaction with just Na^+ channels. *C*, flecainide concentrations acting on only RyRs.

Table 5. Parameters for SR Ca^{2+} release

Parameter Name	*Value / Units*
k_{on}	[D+]*Diffusion
k_{off}	0.011
Diffusion	5500 $M^{-1}ms^{-1}$
k_s	25 ms^{-1}
k_{oCa}	10 $mM^{-2}ms^{-1}$
k_{om}	0.06 ms^{-1}
k_{iCa}	0.5 $mM^{-1}ms^{-1}$
k_{im}	0.005 ms^{-1}
$EC_{50\text{-}SR}$	0.45 mM
Max_{SR}	15
Min_{SR}	1
H_{SR}	2.5
K_{SRleak}	5.348e-6 ms^{-1}

concentration–response relationship with a Hill coefficient of 1 ($n = 1$) as follows:

$$G_{IKr} = G_{IKr,max} \times \left(\frac{1}{1 + \left([Drug]/IC_{50} \right)^{n}} \right)$$

where $G_{IKr,max}$ is the nominal conductance value from the given rabbit ventricular myocyte model (Soltis & Saucerman, 2010) and IC_{50} is the concentration of drug that produces a 50% inhibition of I_{Kr} current. The IC_{50} values for the drug to inhibit I_{Kr} current are for flecainide 1.5 μM (Belardinelli *et al.* 2013) and for ranolazine 12 μM (Rajamani *et al.* 2008).

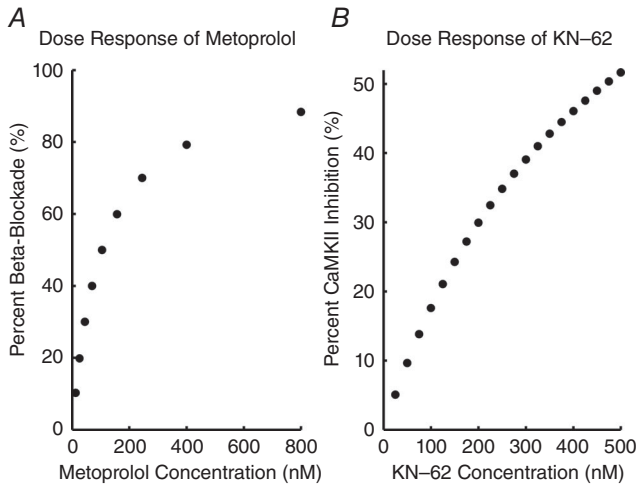

Figure 2. Dose–response curves for metoprolol on β_1-receptor blockade and KN-62 on CaMKII inhibition
A, dose–response curves for the effect of metoprolol on β-adrenergic activity were extracted from an experimental model (Abrahamsson *et al.* 1990). *B*, dose–response data were obtained from (Davies *et al.* 2000) and fitted to a percentage block of CaMKII for given doses of KN-62.

Simulation of effect of metoprolol on β-adrenergic activity and CaMKII blocking effects of KN-62

We modelled the β_1 and CaMKII blocking effects of metoprolol ($IC_{50} = 105$ nM) and KN-62 ($IC_{50} = 468$ nM) as a competitive inhibitor of β-agonist and limiter of free endogenous total CaMKII, respectively. Dose–response curves (Fig. 2) for the effect of metoprolol on β-adrenergic activity were extracted from an E_{max} experimental model (Abrahamsson *et al.* 1990), where the percentage inhibition of E_{max} represents the fraction of ISO inhibition. In preliminary tests of the computational model involving myocyte pacing, 50 nM ISO achieved 98% of the maximal response to agonist; ISO inhibition was therefore modelled as a percentage of 50 nM applied ISO. Thus, in Fig. 2*A*, percentage β_1-receptor blockade refers to the percentage of β_1-receptors that are competitively blocked by metoprolol. KN-62 was modelled as an inhibitor of endogenously available CaMKII (Tokumitsu *et al.* 1990). Dose–response data were obtained from Davies *et al.* (2000) and fitted to a percentage block of CaMKII for given doses of KN-62; similarly, percentage CaMKII inhibition in Fig. 2*B* refers to the percentage of endogenous CaMKII that is inhibited by KN-62. Data are from Abrahamsson *et al.* (1990) (metoprolol) and Tokumitsu *et al.* (1990) (KN-62). We applied the E_{max} model from Abrahamsson *et al.* (1990) to determine our dose–response relation as follows:

$$\%\ \beta - \text{Blockade or \% CaMKII inhibition} = \frac{E_{max} \times C}{IC_{50} + C}$$

where $E_{max} = 100\%$, and C is the metoprolol or KN-62 concentration.

CPVT CASQ2(−/−) model development

The CPVT phenotype was modelled via a computational CASQ2(−/−) (Knollmann *et al.* 2006) by modifying the Soltis–Saucerman model (Soltis & Saucerman, 2010). We set the calsequestrin buffer concentration and the time derivative of the calsequestrin buffer concentration to 0. While this has no direct effect on regulating RyR2 function, it was expected to still demonstrate a functional effect on RyR2 activity because of alterations to intracellular SR Ca^{2+}. Equations for the regulation of Na^+/K^+-ATPase activity by PKA as mediated by phospholemman were incorporated from the Yang–Saucerman model (Yang & Saucerman, 2012). Our previously validated Na^+ channel (Moreno *et al.* 2011) and modified RyR2 channel were inserted into the cellular model (Soltis & Saucerman, 2010).

Stochastic single channel RyR2 simulations

Individual RyR2 channels were modelled stochastically in Monte Carlo simulations using Gillespie's algorithm (Gillespie, 1977). Parameters were constrained by fixed concentrations of flecainide (0 and 50 μM), luminal Ca^{2+} (1 mM), and junctional Ca^{2+} (0.1 μM), mimicking experimental conditions (Hwang *et al.* 2011). Stochastic error diminishes over a large number of simulations, approaching the expected mean open time (T_o), mean closed time (T_c), and open probability (P_o) as derived by the methods of Colquhoun & Hawkes (1981).

Cellular and tissue simulations

Mouse ventricular myocyte model. The I_{Na} channel was replaced in the Morotti–Grandi mouse cardiac cell model (Morotti *et al.* 2014) with our published Markov model (Moreno *et al.* 2013). We then adjusted three transition rates for the mouse model to simulate the mouse I_{Na} kinetics as follows: O→C1, $\beta_{13} \times 0.45$; O→IF, $\alpha_2 \times 0.45$; O→IS, $\alpha_x \times 0.45$. Virtual myocytes were paced using a -9.5 pA pF^{-1} current stimulus for 5 ms in single cells for 150 s at 2 Hz pacing frequency in the presence and absence of drug and 0.5 μM isoproterenol (ISO).

Rabbit ventricular myocyte model. Virtual whole cells and tissues (both WT and KO) were allowed to 'rest' without external stimuli for 10 min to establish initial conditions. Cells were then virtually paced (using a -80 pA pF^{-1} current stimulus for 0.5 ms in single cells and -500 pA pF^{-1} stimulus for 2.0 ms in tissues) for 5 min at specific pacing frequencies in the absence of drug or agonist. Cells were finally paced for an additional 2 min in the presence and absence of drug and 1 μM ISO. Parameters including upstroke velocity, action potential duration (APD) and the number of early and delayed afterdepolarizations (EADs and DADs) were tracked over the course of each simulation.

One-dimensional (1D) tissue was simulated as a fibre of 165 cells (1.65 cm) (Glukhov *et al.* 2010) with reflective boundary conditions. Transmural heterogeneity was incorporated into the tissue by a linear decrease to 25% maximal I_{to} conductance (Myles *et al.* 2010), corresponding to a linear transition from epicardial to endocardial tissue (Fedida & Giles, 1991) and an APD gradient of 205–224 ms. The diffusion coefficient D_x was set to 0.002 cm^2 ms^{-1} to establish a conduction velocity of 61–73 cm s^{-1} (epicardium–endocardium in WT conditions) (Brugada *et al.* 1990).

Code for simulations and analysis was written in C++ and MATLAB 2014a (The Math Works, Inc., Natick, MA, USA). Code was run on an Apple Mac Pro machine with two 2.93 GHz 6-Core Intel Xeon processors, and an HP ProLiant DL585 G7 server with a 2.3 GHz 48-core AMD Opteron processor. Code was compiled with the Intel ICC compiler 2013. Numerical results were visualized using MATLAB R2014b. All source code used in this paper is available online or can be obtained by emailing ceclancy@ucdavis.edu.

Results

We modelled the interaction between flecainide and RyR2 by modifying the Shannon–Bers model of the cardiac RyR2 channel (Shannon *et al.* 2004) (see Methods) that reproduces gain and fractional SR Ca^{2+} release, and includes regulation by both luminal and junctional Ca^{2+} fractions. Based on experimental data, drug binding was modelled as voltage-independent open-state block that results in a ~20% subconductance state (Hilliard *et al.* 2010; Hwang *et al.* 2011; Mehra *et al.* 2014). A different recent study suggested that flecainide does not block the RyR (Bannister *et al.* 2015). These effects are also included in the cellular level simulations as no RyR block by flecainide.

This assumption resulted in predictions of drug effects that were consistent with experiments in single channel lipid bilayer studies (Hilliard *et al.* 2010). Stochastic Monte Carlo simulations reveal intermittent closures that interrupt channel openings, corresponding to flecainide binding and unbinding the open-state (Fig. 3*A*) (Hwang

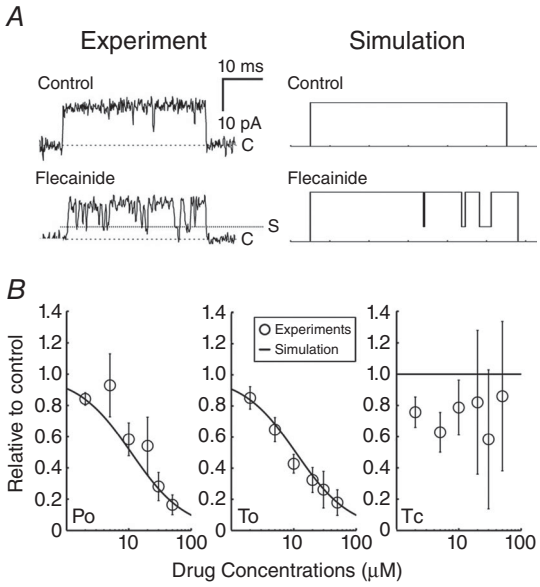

Figure 3. Simulated interaction of flecainide with single ryanodine receptors
A, experimental single RyR channels in bilayers (left) compared with stochastic model simulations (right), in the absence (top) and presence (bottom) of 50 μM flecainide. *B*, measured and simulated dose dependence of flecainide on channel open probability (P_o, left), mean open time (middle, T_o), and mean closed time (T_c). Experimental data points (circles) and simulated results from ~1,000,000 stochastic openings and closures at concentrations as indicated (lines). Experimental data are from Hilliard *et al.* (2010 and Hwang *et al.* (2011).

et al. 2011). Figure 3*B* shows model predictions (lines) closely match experimental measurements (symbols) of drug concentration-dependent effects on channel open probability (left) and channel mean open time (middle) (Hwang *et al.* 2011). Mean closed time displays no dose dependence in this binding scheme, as in experimental findings (Fig. 3*B*, right). We modelled flecainide interactions with the Na^+ and hERG K^+ channel as described previously (Moreno *et al.* 2011) (Moreno *et al.* 2013).

We generated a virtual calsequestrin knockout mouse cardiac myocte (CASQ2(−/−)) by setting the concentration of CASQ to zero in the Morotti–Grandi model of the mouse ventricular myocyte, which includes the β-adrenergic signalling and CaMKII pathways (Morotti *et al.* 2014). We then predicted the effects of the virtual CASQ2(−/−) on electrical and Ca^{2+} dynamics. Figure 4*A–D* shows action potentials (APs) (top) and Ca^{2+} transients (bottom) of cells paced at a frequency of 2 Hz. As expected, the Ca^{2+} transient amplitude increases upon application of 0.5 μM isoproterenol (ISO) (Fig. 4*B*). In the absence of ISO, CASQ2(−/−) myocytes demonstrate reduced but intact Ca^{2+} transients and APs compared with control (compare Fig. 4*C* to Fig. 4*A*) consistent with experimental observations in CSQN mutant and CSQN underexpression mouse myocytes (Viatchenko-Karpinski *et al.* 2004; Terentyev *et al.* 2008; Gyorke & Terentyev, 2008). Consistent with multiple experimental observations, application of 0.5 μM ISO induces spontaneous Ca^{2+} release events (red arrows Fig. 4*D*, bottom), which drive afterdepolarizations (Knollmann *et al.* 2006; Gyorke & Terentyev, 2008; Hilliard *et al.* 2010; Liu *et al.* 2013). Following development of the virtual mouse model of CPVT, which is validated by many published experimental data, we generated a virtual calsequestrin rabbit knockout (CASQ2(−/−)). This approach allows for cross species testing, e.g. to predict how larger animals (more 'human-like') would respond, and to also look for model independence of our findings.

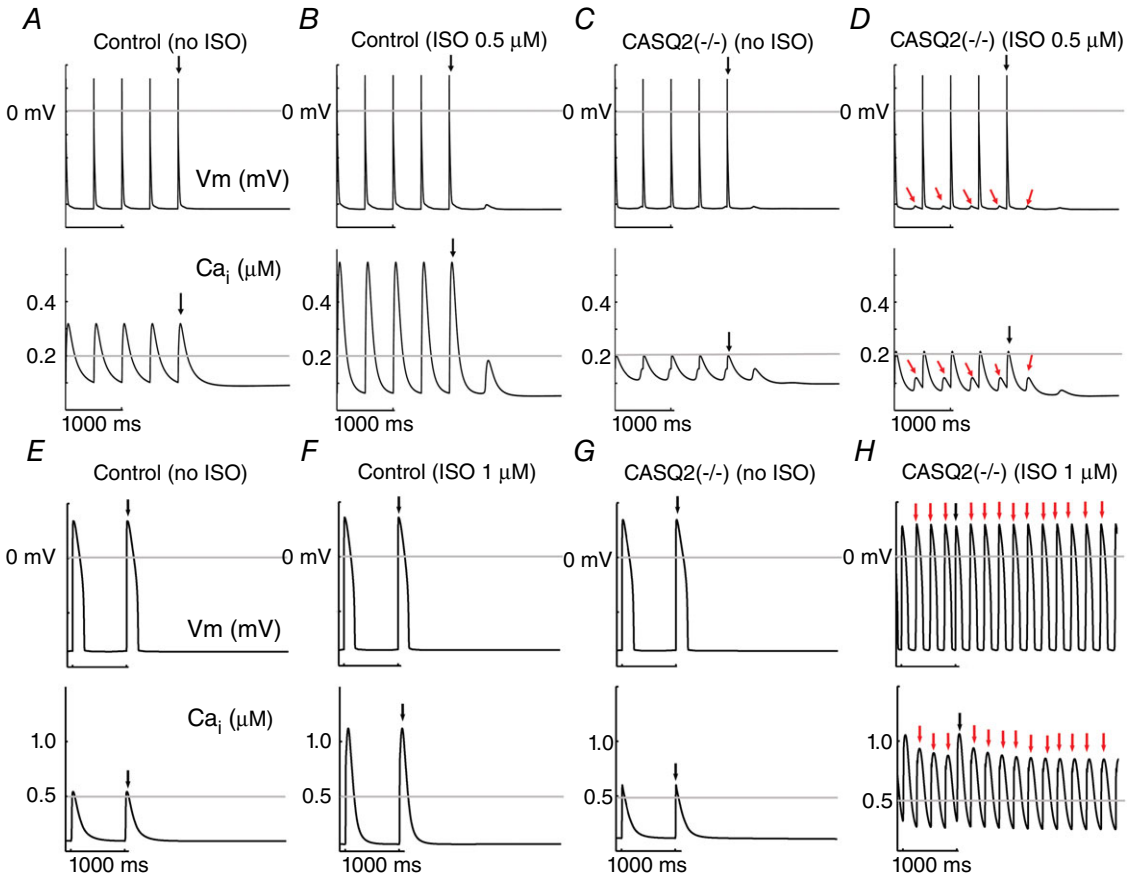

Figure 4. An *in silico* calsequestrin (CASQ2(−/−)) knockout model recapitulates the CPVT phenotype
In each panel, simulated membrane voltage (top) and intracellular Ca^{2+} transients (bottom) are shown during 2 Hz pacing in the mouse virtual myocyte (*A–D*) and 1 Hz in the rabbit virtual myocyte (*E–H*). *A*, simulated control mouse ventricular myocytes. *B*, control mouse cell with 0.5 μM simulated isoproterenol (ISO). *C*, simulated CASQ2 knockout mouse. *D*, 0.5 μM ISO applied to the simulated CASQ2 knockout mouse. *E*, simulated control rabbit ventricular myocytes. *F*, control rabbit cell with 1 μM simulated isoproterenol (ISO). *G*, simulated CASQ2 knockout rabbit. *H*, 1 μM ISO applied to the simulated CASQ2 knockout rabbit. Red arrows indicate spontaneous triggers. Black arrow is the final stimulus.

The rabbit model was constructed by setting the concentration of CASQ to zero in the Soltis–Saucerman model of the rabbit ventricular myocyte, which contains the β-adrenergic signalling and CaMKII pathways. Figure 4*E–H* shows simulated rabbit APs (top) and Ca^{2+} transients (bottom) of control cells paced at a frequency of 1 Hz. As observed in the mouse model, the Ca^{2+} transient amplitude increases upon application of 1 μM ISO (Fig. 4*F*). In the absence of ISO, CASQ2(−/−) myocytes demonstrate morphologically similar Ca^{2+} transients and APs to control (compare Fig. 4*G* to Fig. 4*E*). No differences were found with other pacing frequencies. Consistent with experimental observations (Kornyeyev *et al.* 2012), application of 1 μM ISO induces spontaneous Ca^{2+} release events (red arrows Fig. 4*H*, bottom), which drive depolarizations that trigger APs (red arrows in Fig. 4*H*, top).

Recent publications have suggested that flecainide may be insufficiently concentrated inside the cell to affect the RyR directly (Liu *et al.* 2011*a*, 2012). Thus, we employed a novel atomic scale modelling approach to compute free energy profiles for flecainide transport in the extracellular, membrane and intracellular compartments (Fig. 5*A*).

With a pK_a value of 9.8, 97% of flecainide will exist in the protonated form at physiological pH. However, recent studies suggest that the hydrophobic environment of the lipid bilayers promotes stabilization of the neutral form, allowing for flecainide entry upon deprotonation. To assess feasibility of this mechanism, we determined

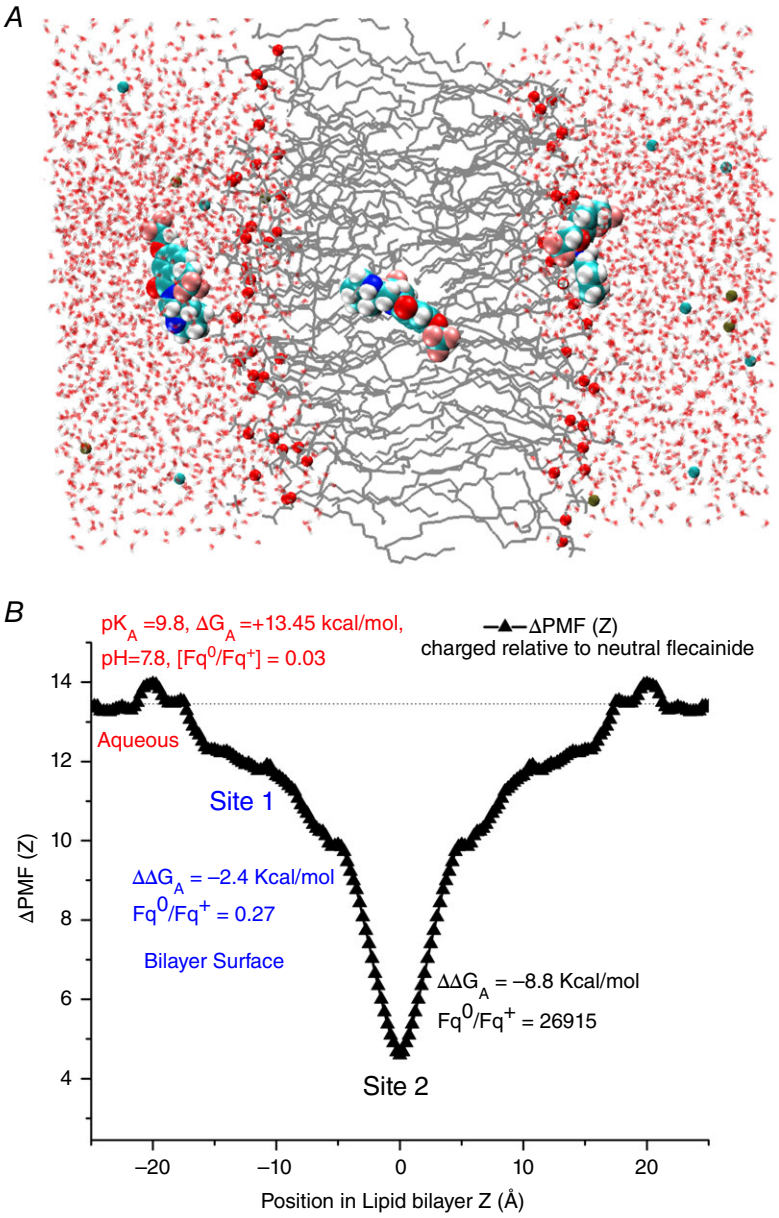

Figure 5. Atomic scale prediction of flecainide transport across the membrane
A, visualization of flecainide transport. *B*, the difference between the potentials of mean force (ΔPMF (*Z*)) across the bilayer, and position-dependent free energies for charged and neutral flecainide ($\Delta\Delta G_A$) at the membrane interface (site 1) and hydrophobic core of the bilayer (site 2). Relative fractions of neutral to charged drug (Fq^0/Fq^+) in the aqueous solution (red), site 1 (blue) and site 2 (black) are shown.

the underlying thermodynamics governing flecainide movement on the surface and in the hydrophobic core of the membrane and the barriers associated with transport of cationic or neutral forms.

Force (PMF) (or Potential mean force free energies (ΔG_A)) for partitioning of charged and neutral flecainide

Both forms of flecainide display preference for interfacial partitioning with stabilization of about 8 and 11 $k_B T$ for charged and neutral flecainide, respectively. The simulations show that concentration of neutral flecainide will increase substantially on the surface as compared to the bulk phase and will be predominant in the hydrophobic core of the bilayer (site 2). There is a substantial penalty for protonated drug to cross a hydrophobic core, although it will act as a sink for a neutral flecainide with a very small crossing barrier for the drug ($\sim 2k_B T$ not shown).

The difference between the potentials of mean force (ΔPMF (Z)) across the bilayer, and position-dependent free energies for charged and neutral flecainide ($\Delta\Delta G_A$) at the membrane interface (site 1) and hydrophobic core of the bilayer (site 2) are shown in Fig. 5*B*. We calculated the pK_a shift due to drug deprotonation upon partitioning into lipid bilayers from the difference between the position-dependent free energies for charged and neutral flecainide ($\Delta\Delta G_A$).

$$\Delta\Delta G_{\text{deprot}} = W_{\text{Flec}^0}(z) - W_{\text{Flec}^+}(z)$$

$$\Delta \text{p}K_A = \frac{\Delta\Delta G_{\text{deprot}}}{2.3\ k_B T}$$

ΔpK_a values are also indicated as relative fractions of neutral to charged drug (Fq^o/Fq^+) in the aqueous solution (red), site 1 (blue) and site 2 (black) in Fig. 5*B*. The pK_a shift is close to zero in the bulk (as expected) and then sharply drops at site 1. This indicates that flecainide will readily lose its proton in the membrane environment.

Is diffusion of neutral flecainide sufficient for effective accumulation? We estimated diffusion coefficients from local friction factors along the reaction coordinate in free energy simulations (from fluctuations in the constraining force) (Boggara & Krishnamoorti, 2010). The diffusion coefficient for flecainide was calculated as $\sim 4.9 \times 10^{-7}$ cm^2 s^{-1} in the bilayer, about an order of magnitude lower than bulk water similar to previously reported values for various drugs (Boggara & Krishnamoorti, 2010). Flecainide is predicted to undergo extremely rapid equilibration.

We next predicted the effects of flecainide on control and CASQ2(−/−) rabbit ventricular myocyte models for clinically relevant frequencies at a high therapeutic dose of flecainide (2 μM). In order to map the action potential (AP) dynamics–frequency relationship for the CPVT CASQ2(−/−) with flecainide, the maximum values of the voltage following the upstroke of the AP were collected during the second half of a 2 min simulation and binned vertically for each constant pacing frequency; for clarity, only steady state behaviour is shown (t = 60–120 s). In the control simulation there was a stimulus to AP ratio of 1:1 (Fig. 6*A*). The time course of AP at 2 Hz (grey line) is shown on the left (Fig. 6*A*, *C*, *E*, *G* and *I*). The peak of the calcium transient was similarly monitored (control – Fig. 6*B*), with the time course of the calcium transient at 2 Hz (grey line) in the left of each of the right panels (Fig. 6*B*, *D*, *F*, *H* and *J*).

In the absence of drug, CASQ2(−/−) myocytes displayed triggered APs at frequencies greater than 0.95 Hz (notice the horizontal line in the plot at frequencies slower than 0.95 Hz, corresponding to a stimulus to AP ratio of 1:1), when challenged by 1 μM ISO (Fig. 6*C*). Pathological electrical activity was preceded by spontaneous Ca^{2+} release events from the RyR2 (Fig. 6*D*), which, when resulting in a sufficient release of Ca^{2+}, can integrate in time to induce electrogenic forward-mode sodium–calcium exchange current (3 inward Na^+/1 outward Ca^{2+}) and depolarize the cell, ultimately activating I_{Na}.

Application of a high therapeutic dose flecainide (2 μM), acting on the rabbit RyR2, I_{Kr} and I_{Na} rectified the electrical activity at all frequencies tested (Fig. 6*E*). The electrical stability coincided with suppression of diastolic Ca^{2+} release, but was also accompanied by a markedly reduced Ca^{2+} transient (Fig. 6*F*). The therapeutic range of plasma concentrations for flecainide is 0.5–2.0 μM (Brunton *et al.* 2010). We examined the cases of 0.5, 1.0 and 1.5 μM flecainide acting on each of the targets under the influence of 1 μM isoproterenol, over a range of clinically relevant pacing frequencies, from 0.5 to 3.0 Hz (30–180 beats min^{-1}; Leenhardt *et al.* 1995), at 0.01 Hz increments (Fig. 7). Low dose flecainide (0.5 μM) failed to suppress Ca^{2+} alternans, a marker of proarrhythmia (Chudin *et al.* 1999), which emerged at frequencies greater than 1.6 Hz and suggests incomplete efficacy in the lower range of therapeutic dosing (Fig. 7*A*).

We next simulated drug action on the Na^+ current or RyR *alone* to determine the contributions of each target to drug efficacy. The rabbit model predicted that neither the high dose of flecainide (2 μM in Fig. 6*G* and *H*), nor any lower concentrations, when tested on Na^+ current alone, eliminated pathological activity at all pacing frequencies (Fig. 7*B*). As expected from flecainide's use-dependent blocking behaviour of I_{Na}, higher concentrations and faster pacing frequencies eliminated some arrhythmogenic behaviour, but DADs and triggered action potentials persisted. Derangement of Ca^{2+} activity also persisted, and was largely unaffected by drug effects on the Na^+ current (Fig. 6*H*).

Selective application of flecainide on RyR2 yielded results comparable to the case flecainide acting on both targets (compare Fig. 6*I* and *J* (selective RyR2) with Fig. 6*E* and *F* (both targets)). Mid- and high-dose flecainide acting on the RyR2 alone resolved pathological behaviour at the cellular level, though Ca^{2+} alternans and DADs still emerged at lower doses (Fig. 7*C*).

We next modelled the physiological effects of acute application of isoproterenol on heart rate, mimicking acute sympathetic stimulation. In Fig. 8, rabbit cells were paced to steady-state (for 500 s) at 1 Hz and then subjected to isoproterenol and an increase in pacing frequency (cycle length = 600 ms). Compared with control virtual cells that responded uneventfully to sympathetic challenge (Fig. 8*A*), the virtual CASQ2(−/−) CPVT mutation generated multiple spontaneous APs, observed in the histogram of peak voltages in time (left side of left panels) and in the time course of the membrane potential (right of left panels during the time indicated by the boxed region in the left panels). As observed for steady-state pacing, simulated 2 μM flecainide application on both the Na^+ current and RyR (Fig. 8*C*) normalized aberrant behaviour, while flecainide effects on the Na^+ channel alone were insufficient (Fig. 8*D*). A dose of 2 μM flecainide acting on the RyR alone normalized the membrane potential and prevented spontaneous Ca^{2+} release (Fig. 8*E*). We also tested different pacing cycle lengths from 300 ms to 500 ms, and found similar results (data not shown).

We next predicted the effects of flecainide in a rabbit one-dimensional (1D) transmural heterogeneous tissue. Stimulation was applied to the endocardial site of the CASQ2(−/−) rabbit tissue at 2 Hz (120 beats min^{-1}) with 1 μM ISO, in the presence or absence of flecainide. Spontaneous Ca^{2+} releases from the RyR2 often resulted in sufficient calcium loading to drive inward I_{NCX}, causing DADs that were occasionally sufficient in amplitude to activate Na^+ channels for a triggered AP (red arrows – Fig. 9*A*).

Flecainide at 2 μM acting on both the Na^+ channels and the RyRs suppressed propagated arrhythmogenic activity by regulating underlying SR Ca^{2+} release (Fig. 9*B*). Also consistent, 2 μM flecainide acting on I_{Na} alone did not prevent spontaneous Ca^{2+} release and DADs (Fig. 9*C*). However, 2 μM flecainide acting on the

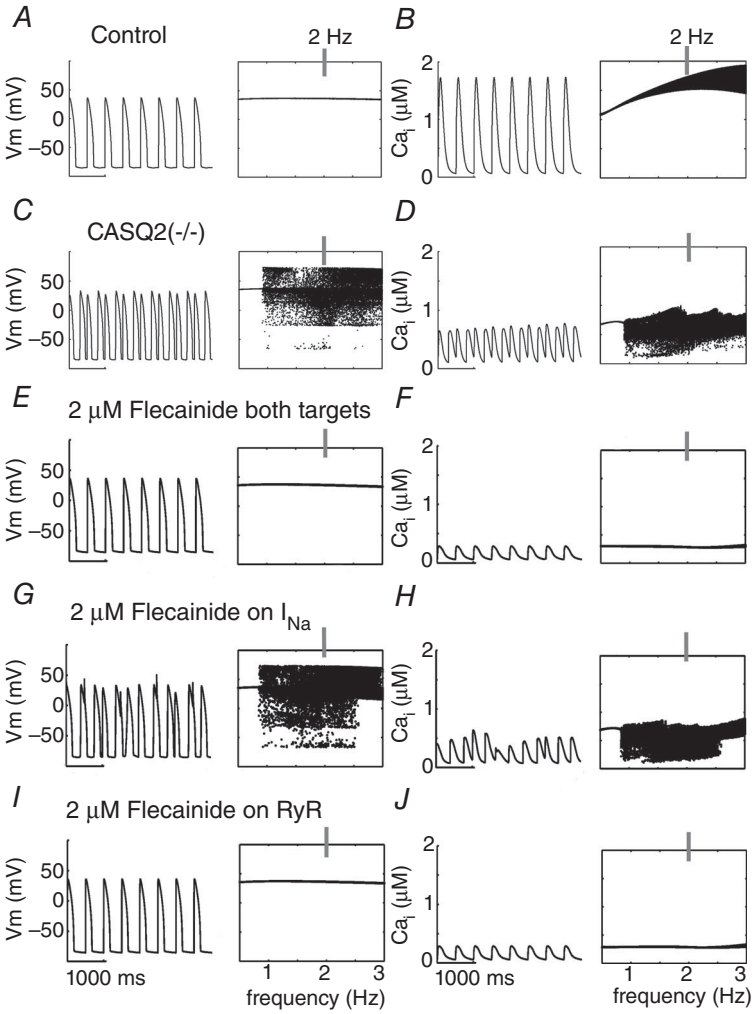

Figure 6. Model prediction of flecainide mechanism
The time course of action potentials is in left columns and calcium transients (CaTs) in right columns at 2 Hz. Voltage and Ca^{2+} transient dynamics over a range of physiological frequencies is shown to the right of each simulated time course at 2 Hz: the voltage maxima are binned for each pacing frequency between 0.5 and 3 Hz during the second half of a 2 min simulation time course. *A* and *B*, control APs, CaTs. *C* and *D*, CASQ2(−/−) APs, CaTs. *E* and *F*, CASQ2(−/−) myocyte APs and CaTs with high clinical dose (2 μM) flecainide effects on both Na^+ channels and RyRs. *G* and *H*, high dose flecainide acting only on Na^+ channels. *I* and *J*, high dose flecainide (2 μM) on only RyRs.

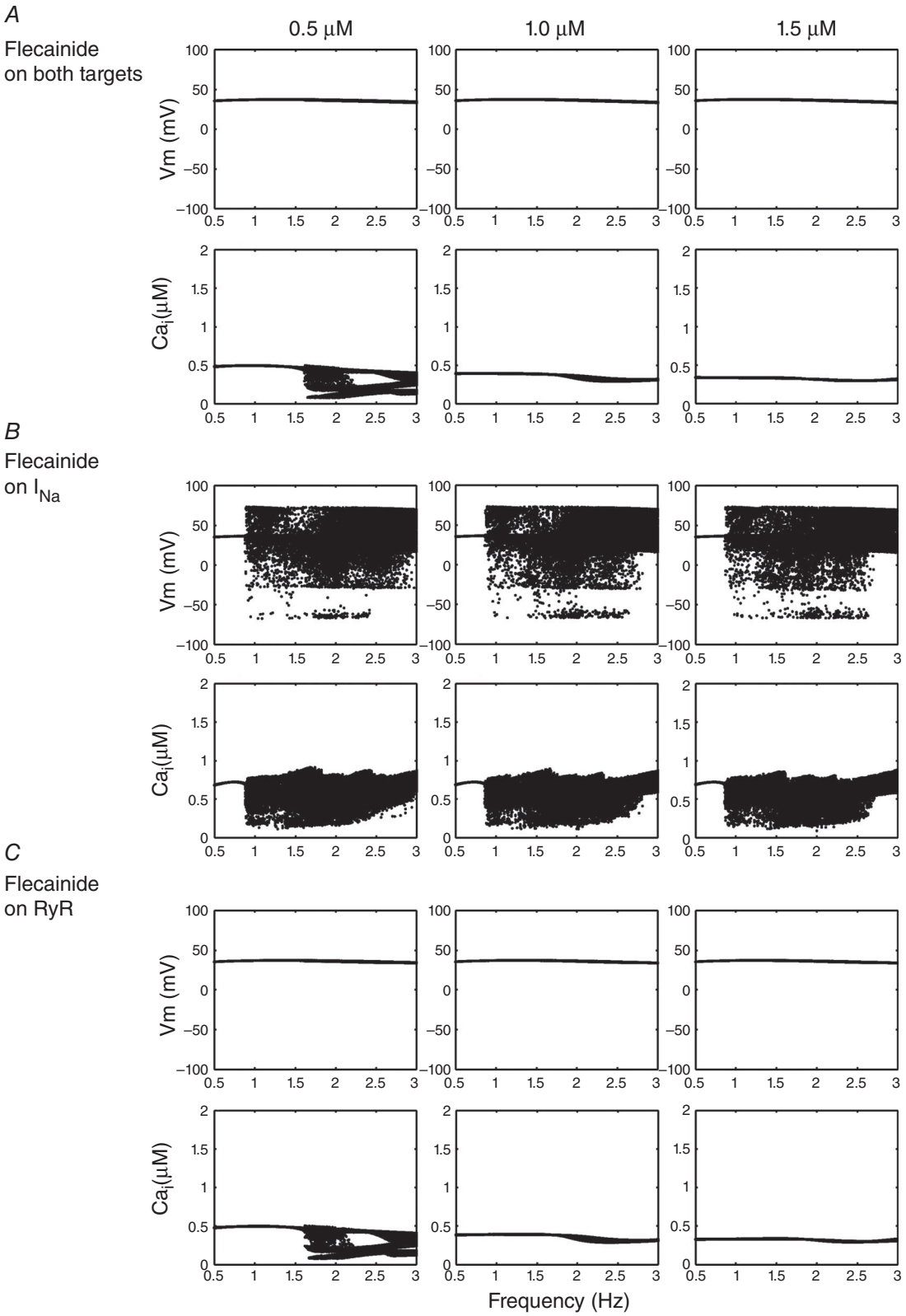

Figure 7. Full parameter space of flecainide efficacy for I_{Na}, RyR2 and both targets in combination
Voltage dynamics is shown for each flecainide case, and the voltage and Ca^{2+} transient maxima are binned for each pacing frequency between 0.5 and 3 Hz during the second half of a 2 min simulation time course. *A*, CASQ2(−/−) myocytes with 0.5, 1.0 and 1.5 μM flecainide effects on both Na^+ channels and RyRs. *B*, flecainide concentrations acting on only Na^+ channels. *C*, flecainide interaction with just RyRs.

RyR2 alone was sufficient for therapeutic suppression of DADs and triggered APs (Fig. 9*D*). Notably, 2 μM flecainide acting on I_{Na} (e.g. Fig. 9*B* and *C*) slowed tissue conduction velocity from 66 to 44 cm s^{-1} as compared with 2 μM flecainide acting on RyR2 alone, consistent with well-documented detrimental conduction velocity in coupled tissue (Starmer *et al.* 1991; Moreno *et al.* 2011).

We further probed concentration dependence of our RyR2-specific effects of flecainide, and found strong dose dependence. Subthreshold DADs arising from spatially discordant Ca^{2+} alternans emerged in the presence of 0.5 μM and 0.65 μM flecainide acting on RyR2 (Fig. 10), alone and in combination with I_{Na} block (not shown). Figure 10*B* and *D* show the time course of the Ca^{2+} mediated alternans development for 0.5 μM and 0.65 μM flecainide, respectively, acting on RyR2 alone.

Given the therapeutic potential of flecainide to normalize Ca^{2+} anomalies in the CPVT-linked CASQ2(−/−), we set out to predict whether other Na^+ channel blockers might suppress emergent-triggered activity in rabbit ventricular myocyte models. We simulated the pure Na^+ channel blocker lidocaine (20 μM) and the late Na^+ current/hERG channel blocker ranolazine (5 μM) (Moreno *et al.* 2013). Lidocaine and ranolazine

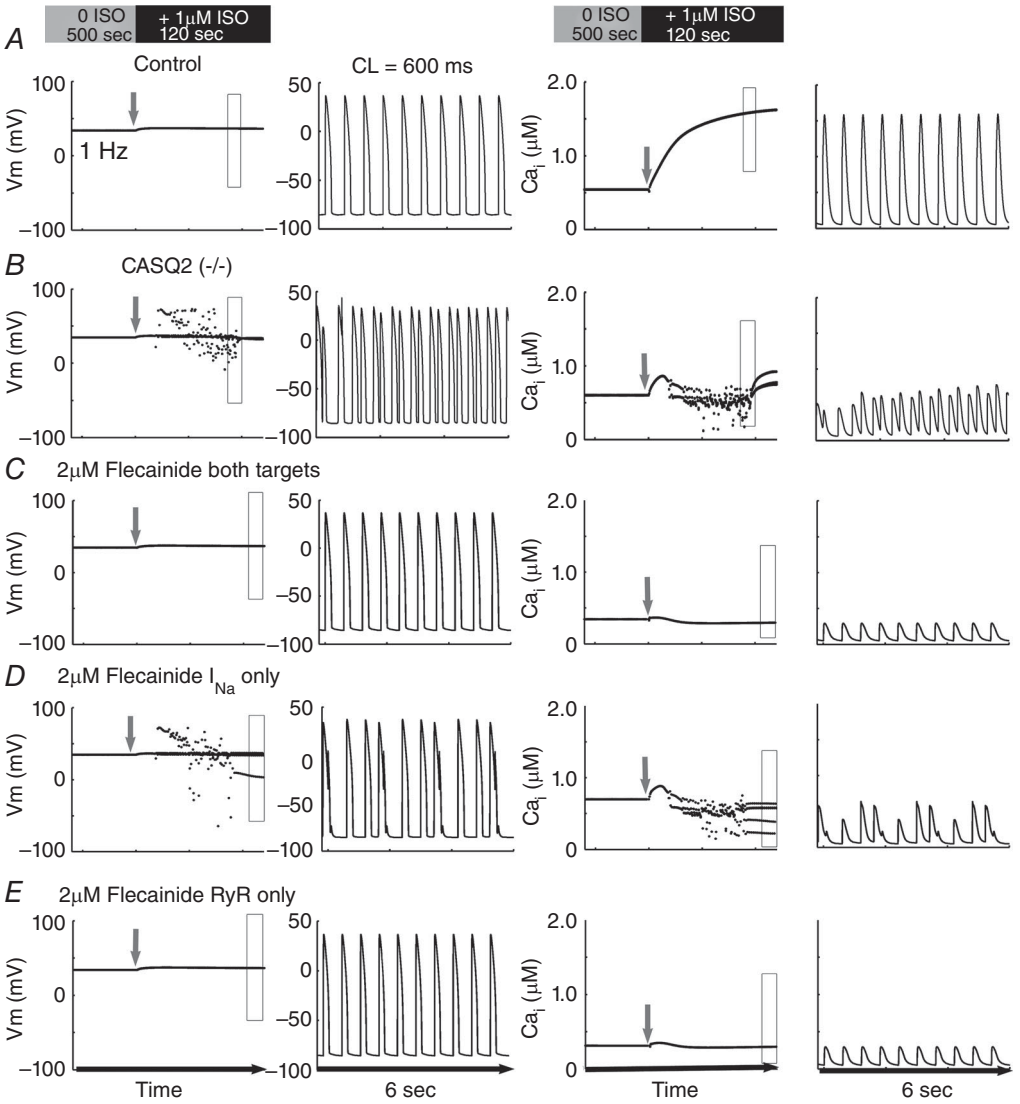

Figure 8. Simulation of the physiological effects of isoproterenol on heart rate
Five hundred beats were paced in control cells at Basic Cycle Length (BCL) 1000 ms (1 Hz) without ISO; cycle length was abruptly decreased to 600 ms with concomitant application of ISO (1 μM). Peak voltages in time are shown in the left columns, and a representative time course (expanded rectangle of left panels) of the membrane potential action potentials is in the 2nd column. Corresponding peak Ca^{2+} transients are in column 3, with a representative time course shown in the far right columns. The grey arrow in each panel denotes onset of pacing acceleration and application of ISO.

have both failed to demonstrate efficacy in the suppression of Ca^{2+} wave formation (Galimberti & Knollmann, 2011). For both lidocaine and ranolazine devoid of RyR2 interaction, our results mimicked selective I_{Na} inhibition by flecainide. Lidocaine (Fig. 11*A*) and ranolazine (Fig. 11*B*) did not prevent spontaneous depolarizations at all frequencies. Protocol is as in Fig. 6.

Low dose flecainide is predicted to be insufficient for normalizing the CASQ2(−/−) CPVT mutation-induced proarrhythmia in simulated cells and tissues. The extension of these results is that high doses may be required for clinical therapy, which may paradoxically promote arrhythmia. β-Blockade is associated with suboptimal management and pronounced side effects. Thus, we set out to utilize modelling and simulation to guide a novel form of virtual pharmacopoeia in an attempt to identify alternative CPVT therapy. We considered combinations of on-market or preclinical drugs that would cumulatively regulate the RyR2 at lower concentrations, and minimize risk associated with off-target interactions of each drug.

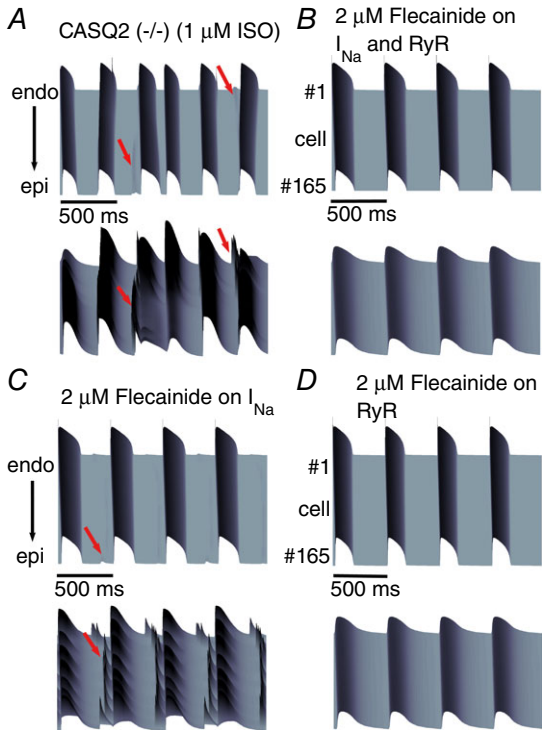

Figure 9. Space–time representations of one-dimensional simulations of flecainide effects on CPVT at BCL 500ms
For each set of panels, voltage time course is on the top, calcium transient is on the bottom. *A*, simulated one-dimensional coupled tissue harbouring the CASQ2(−/−) CPVT mutation in the absence of drug. *B*, effect of flecainide (2 μM) on I_{Na} and RyR. *C*, flecainide (2 μM) effects on I_{Na} alone. *D*, simulated effects of 2 μM flecainide on the RyR alone. Red arrows indicate spontaneous DADs, triggered action potentials and Ca^{2+} transients.

We used the computational model to test the hypothesis that a multidrug combination of flecainide, β-blockade, and CaMKII inhibition would demonstrate efficacy in CPVT. Although little is known about CaMKII inhibition in humans, the signalling molecule regulates many targets and is highly distributed in the brain; thus it is expected that high doses of CaMKII inhibition should be avoided (Ledoux *et al.* 1999; Kaurstad *et al.* 2012). However, both β-blockers and CaMKII inhibitors are classes of drugs that functionally modulate RyR2 activity (Fig. 12*A*), and are suggested to provide efficacy in the management of CPVT (Pott *et al.* 2011; Liu *et al.* 2011*b*; Di Pasquale *et al.* 2013).

We modelled the β_1-blocking effects of metoprolol (IC_{50} = 105 nM) as a competitive inhibitor of β-agonist, and CaMKII inhibition by KN-62 (IC_{50} = 468 nM) as a limiter of free endogenous total CaMKII (see Fig. 2; individual drug efficacy of β-blockade and CaMKII).

We tested in a full factorial combination: the range of relevant concentration combinations in single cells at 2 Hz 0–1 μM flecainide (0.1 μM increments), 0–420 nM metoprolol (corresponding to 0–80% block of β-receptors, at 8% increments), and 0–468 nM KN-62 (corresponding to 0–50% CaMKII inhibition at 5% increments). Among the combinations tested, a combined dose of 0.5 μM flecainide, 70 nM metoprolol and 312 nM KN-62 resulted in controlled Ca^{2+} and voltage activity over the duration of single cell pacing at 2 Hz (Fig. 12*B*). Parameter space maps were generated for the three-drug combination indicating ranges of dose to prevent DAD formation and spontaneous Ca^{2+} release events. Among the 1331 combinations tested, the surfaces shown in Fig. 12*C* represent the efficacy of these combinations on voltage (top row) and spontaneous Ca^{2+} releases (bottom row). When the surface is dark blue, no DADs occurred (voltage), while the dark blue surface in the bottom panels of Fig. 12*C* indicates that no spontaneous Ca^{2+} release events occurred. Even for some drug combinations that remediated DADs, spontaneous Ca^{2+} releases still occurred (indicated by larger blue area in the DAD row than the spontaneous Ca^{2+} release row). The effect of flecainide alone is contained within these graphs where the concentration of the other drugs is zero. The red stars in Fig. 12*C*, right, show one predicted optimal therapeutic combination, a combined dose of 0.5 μM flecainide, 70 nM metoprolol and 312 nM KN-62, resulted in just one effective combination that remediated Ca^{2+} and voltage activity (indicated by a star). This is within a parameter space of local minima, indicating eradication of single cell proarrhythmia event markers (e.g. DADs and spontaneous Ca^{2+} release (SCaR) events).

Finally, we simulated our drug combination of 0.5 μM flecainide, 70 nM metoprolol and 312 nM KN-62 in CASQ2(−/−) in 1D tissue, and compared the results with a simulated tissue pretreated with 0.5 μM flecainide (Fig. 12*D*). Compared with flecainide alone, combination

therapy was superior by (i) requiring a lower dose of flecainide (and thus maintaining conduction velocity 41 cm s^{-1} for flecainide *vs.* 59 cm s^{-1} for combination therapy); (ii) fully suppressing all DADs and triggered APs; (iii) reducing APD_{90}; (iv) normalizing $[Ca]_i$; and (v) preventing the occurrence of spatially discordant Ca^{2+} alternans (see Table 6).

We next tested if the rabbit model prediction for flecainide, β-blockade and CaMKII polytherapy would hold true in the computational mouse model, as a test of the model independence of our findings. Just as we observed for the rabbit model predictions, high dose (2 μM) flecainide effects on both I_{Na} and the RyR normalized the CASQ2(−/−) CPVT phenotype as shown in Fig. 13*A*. Application of flecainide in the mouse model did not affect the amplitude of the Ca^{2+} transients, consistent with experimental observations in the mouse genetic models (Hilliard *et al.* 2010). Also consistent, the effects of high dose (2 μM) flecainide on I_{Na} alone was predicted to be insufficient for normalizing the CASQ2(−/−) CPVT mutation-induced afterdepolarizations and spontaneous Ca^{2+} release events as shown in Fig. 13*B*. However, 2 μM flecainide acting on the RyR2 alone was sufficient for therapeutic suppression of DADs (Fig. 13*C*). Low dose 0.5 μM flecainide acting on I_{Na} and the RyR2 did not ablate spontaneous Ca^{2+} release events as shown in Fig. 13*D*. We also tested if one of the predicted polytherapy combinations that was found to be effective in the rabbit model simulations was also effective in the mouse. The result, shown in Fig. 13*E*, shows that the drug combination of 0.5 μM flecainide, 70 nM metoprolol and 312 nM KN-62 in the mouse CASQ2(−/−) virtual myocyte completely normalized the cellular phenotype.

We next set out to experimentally test if the model prediction for flecainide, β-blockade and CaMKII polytherapy would be effective in the R176Q/+ CPVT experimental mouse model, an alternate CPVT genotype. The results are shown in Fig. 14. A knock-in R176Q/+ CPVT mouse model was used (six R176Q/+, two WT).

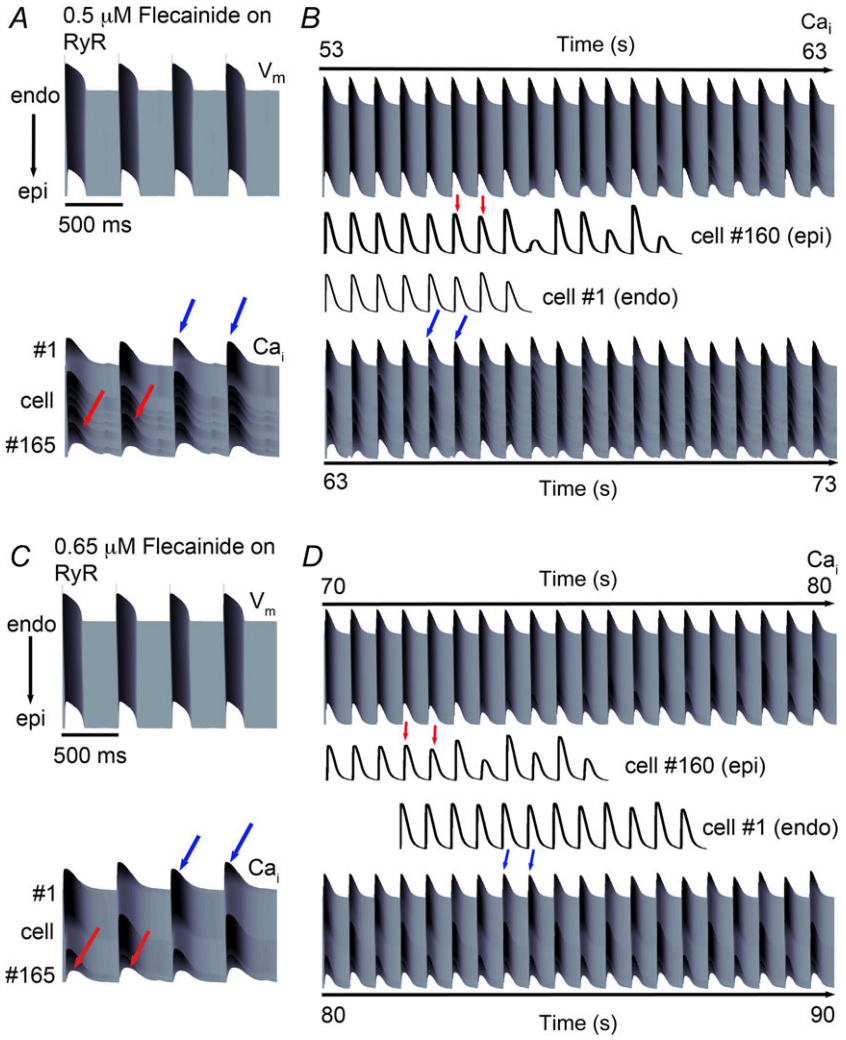

Figure 10. Simulated effects of low clinical dose flecainide effect on RyR only in CPVT one-dimensional tissue
Ca^{2+} alternans developed slowly over time, originating from the epicardial end (red arrows) and continued to the endocardium (blue arrows). *A*, simulated effects of low clinically relevant dose of 0.5 μM flecainide acting on the RyR alone on action potentials (top) and Ca^{2+} transients (bottom). *B*, spatially discordant Ca^{2+} alternans emerge over time. Red arrows correspond to epicardial (Epi) Ca^{2+} alternans, while blue arrows correspond to endocardial (Endo) Ca^{2+} alternans. Cell no. 160 (Epi) is shown from the time 53 s (bottom), and Cell no. 1 (Endo) is shown from the time 63 s (top). *C*, a modest increase in flecainide (0.65 μM) decreased the transient amplitude difference between beats and prolonged the onset of alternans. *D*, extended time course of Ca^{2+} alternans development for 0.65 μM flecainide on the RyR alone. Cell no. 160 (Epi) is shown from the time 70 s (bottom), and Cell no. 1 (Endo) is shown from the time 80 s (top). In panels *B* and *D*, arrows mark the first instance of alternans, which persist for the duration of the simulation.

R176/+ mice develop bidirectional ventricular tachycardia (VT) with catecholamine provocation. At baseline, neither the WT nor the R176Q/+ mice demonstrated ventricular arrhythmias and average heart rate was 462 beats min^{-1} (R176Q/+) and 574 beats min^{-1} (WT) (Table 7). After injection of adrenaline (2 mg kg^{-1} i.p.) and caffeine (120 mg kg^{-1} i.p.), six of six R176Q/+ mice developed bidirectional VT as shown in Fig. 14*A* and *C*. Ventricular tachycardia initiated within 30 s to 6 min and lasted between 1 and 51 min in length (average 21 min) with an average ventricular rate of 807 beats min^{-1}. Both WT and R176Q/+ mice demonstrated T-wave alternans lasting several hours after injection of adrenaline and caffeine. After a 7 day wash-out, the mice were injected with adrenaline and caffeine (2 mg kg^{-1} and 120 mg kg^{-1} i.p., respectively); however, 30 min prior, all mice were given pre-treatment with i.p. injections of flecainide (12 mg kg^{-1}, Sigma-Aldrich), metoprolol (10 mg kg^{-1}, Sigma-Aldrich) and KN-93 (30 μmol kg^{-1}, Calbiochem). All mice demonstrated statistically significant PR, QRS and QTc prolongation 30 min after administration of flecainide, metoprolol and KN-93 (Table 8). Some mice exhibited ST segment changes (data not shown). Heart rates were lower after drug administration but not significantly (Table 8). Adrenaline and caffeine following pre-treatment with flecainide, metoprolol and KN-93 failed to induce ventricular tachycardia in all R176Q/+ mice. Mice demonstrated T-wave alternans (one WT and five R176Q/+) and single premature ventricular contractions (four R176Q/+); however, higher-grade ectopy and the typical bidirectional VT were not seen as shown in Fig. 14*B* and *C*.

Discussion

The optimal pharmacological management of CPVT remains a clinical challenge. The current mainstay of pharmacotherapy often involves maximally tolerated β-blockade despite high (~30–50%) failure rates (Priori *et al.* 2002; Liu *et al.* 2008). In conjunction with pharmacotherapy, mechanical ICD implantation (Miyake *et al.* 2013) and left cardiac sympathetic denervation (Wilde *et al.* 2008) have been used clinically, but carry inherent morbidity and fail to target the mechanistic underpinnings of the CPVT arrhythmia triggers.

While alternative class I antiarrhythmics have been suggested (Galimberti & Knollmann, 2011; Hwang *et al.* 2011), only flecainide has shown moderate clinical success. Its well-studied mechanism of action is inhibition of the inward sodium current (I_{Na}), but data suggest that flecainide interacts with I_{Kr} and RyR2 (Hilliard *et al.* 2010; Galimberti & Knollmann, 2011). Flecainide has demonstrated lethal proarrhythmic effects in other patient populations (Echt *et al.* 1991), and previous clinical failures were largely the result of an incomplete understanding of the emergent proarrhythmic risk.

Recent studies have suggested that because flecainide is 97–99% ionized at physiological pH, it is insufficiently concentrated inside the cell to act on the RyR (Liu *et al.* 2011*a*, 2012), though the study cited as evidence showed the opposite result (Liu *et al.* 2003). The authors made permanently charged flecainide, which when applied intracellularly (via a pipette) led to the same effect as when the same concentration of unadulterated flecainide was applied externally (in the bath). Permanently charged

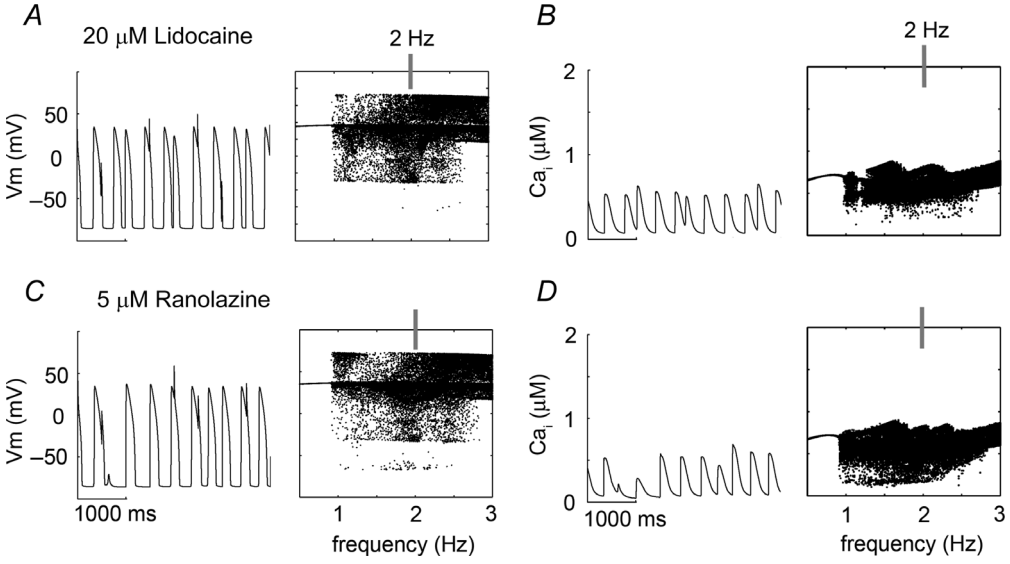

Figure 11. Simulated high clinically relevant doses of lidocaine and ranolazine in CPVT myocytes
Single cell time course is shown at 2 Hz (left) and voltage and calcium transient maxima over a range of frequencies (0.5–3 Hz, right). *A* and *B*, high clinically relevant dose (20 μM) of the pure Na^+ channel blocker lidocaine on voltage and Ca^{2+} transient, respectively. *C* and *D*, clinically relevant dose (5 μM) of the antianginal and late Na^+ current blocker ranolazine on voltage and Ca^{2+} transient, respectively.

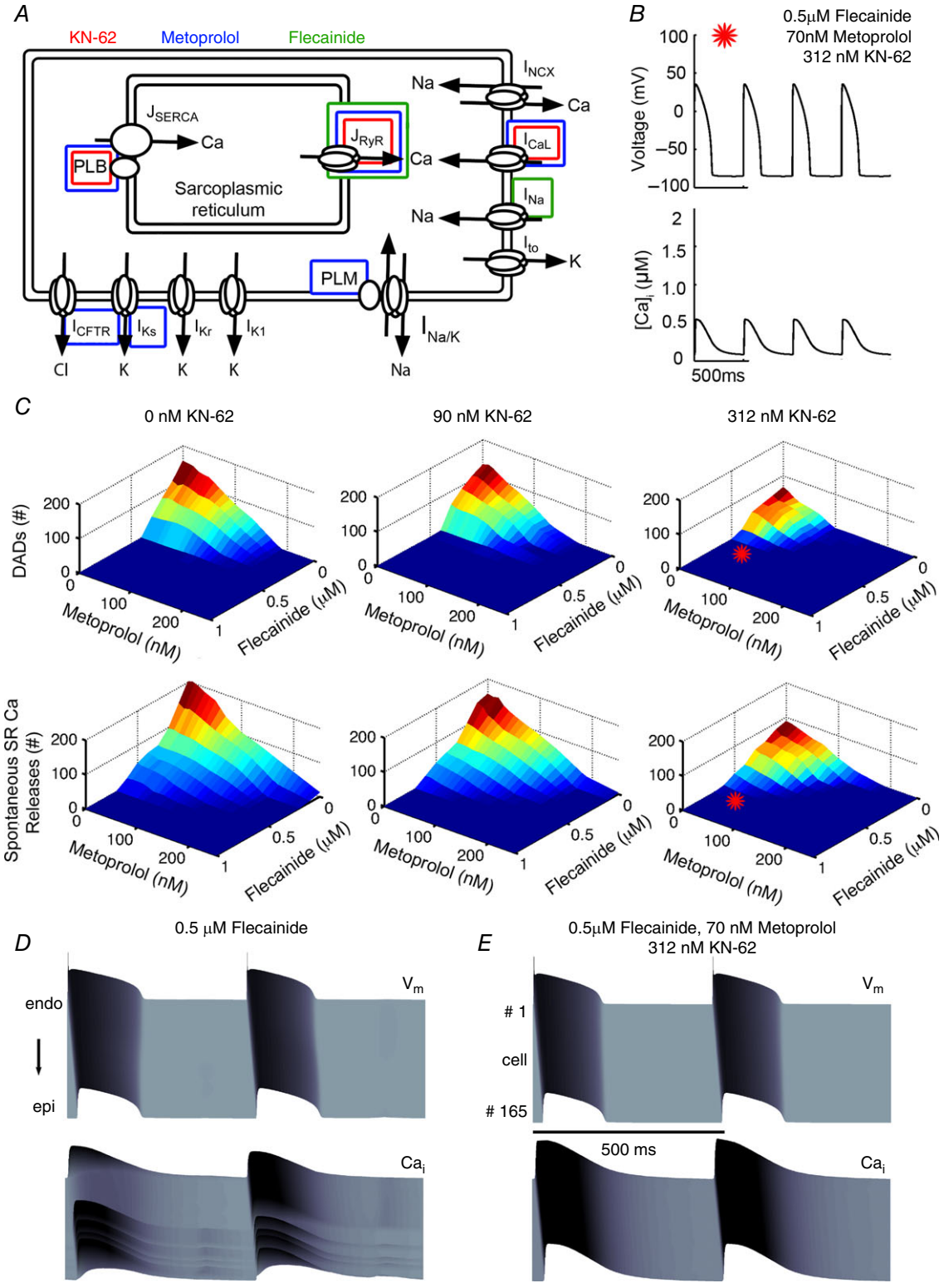

Figure 12. Predicted low-dose polytherapy for CPVT
A, schematic diagram showing the primary targets of flecainide, metoprolol, and KN-62. *B*, prediction of low-dose combined therapy on action potentials (top) and calcium transients (bottom) at 2 Hz *C*, 3 drug combination parameter space simulated in single cells tracking the number of DADs (top) and spontaneous Ca^{2+} releases (bottom). Red stars denote the location of the case in *B* of 0.5 μM flecainide, 70 nM metoprolol and 312 nM KN-62. *D*, simulated tissue effects of low dose flecainide. *E*, predicted tissue effects of combined simulated therapy.

Table 6. CASQ2(−/−) with ISO 1 μM at 2 Hz (rabbit)

Drug concentration	CV (cm s^{-1})	APD_{90} (ms)	$[Ca]_i$ (μM)
Drug free	60	Triggered APs	0.6
Flecainide 2 μM	41	192.5	0.285
Flecainide 0.5 μM + 70 nM Metoprolol + 312 nM KN-62	59	177.8	0.55

flecainide had no effect when applied externally, showing that the drug action cannot be via an extracellular path.

Here, we utilized a physics-based molecular dynamics approach to simulate the partitioning of flecainide by computing free energy profiles for flecainide transport in the extracellular, membrane and intracellular compartments (Fig. 5). The simulations suggest that flecainide accumulates on the membrane surface in

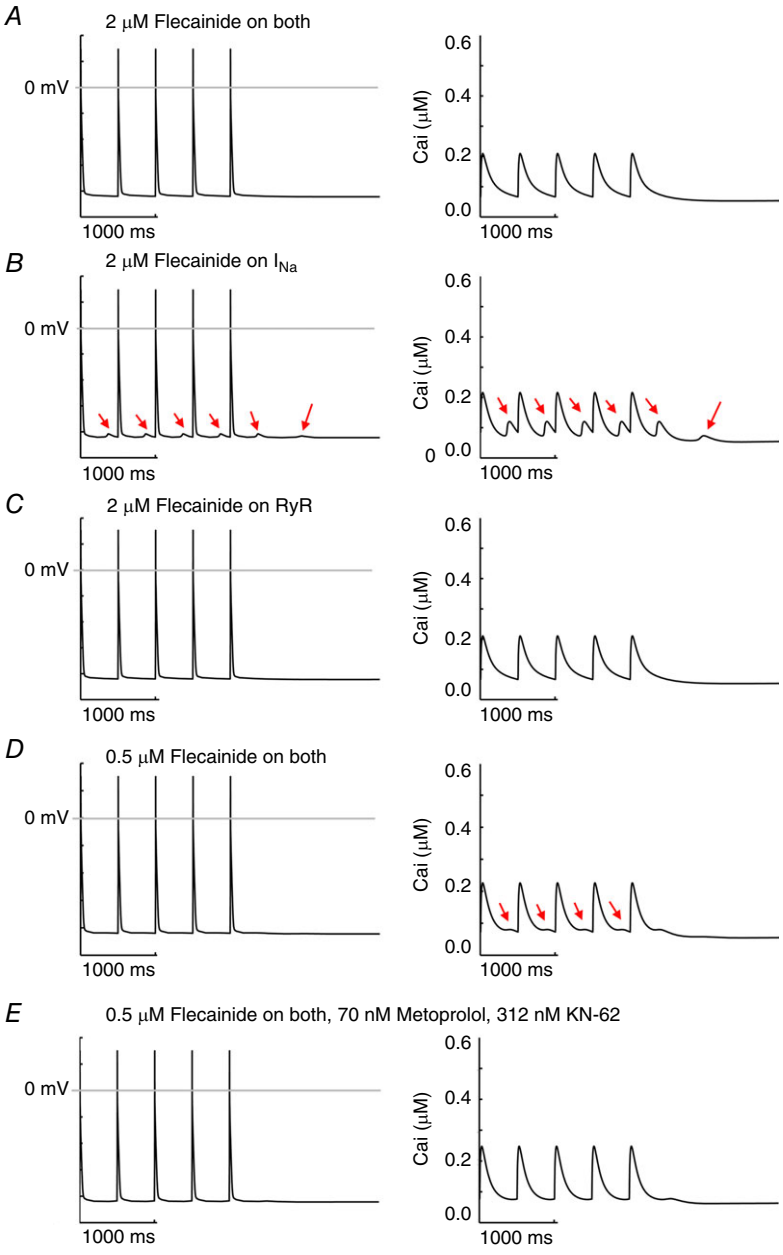

Figure 13. Simulated drug effects in mouse ventricular myocytes
In each panel simulated membrane voltage (left) and intracellular Ca^{2+} transients (right) are shown during 2 Hz pacing. *A*, CASQ2(−/−) myocyte APs and CaTs with high clinical dose (2 μM) flecainide effects on both Na^+ channels and RyRs. *B*, high dose flecainide acting only on Na^+ channels. *C*, high dose flecainide (2 μM) on only RyRs. *D*, low dose flecainide 0.5 μM on both Na^+ channels and RyRs. *E*, simulated test of predicted polytherapy in mouse ventricular myocytes.

cationic and neutral forms after which deprotonation occurs at the surface binding site and promotes membrane crossing down the concentration gradient. The drug then reacquires a proton once it is in the intracellular milieu. This process is extremely rapid, occurring with a diffusion coefficient of $\sim 10^{-7}$ cm s^{-1}, only an order of magnitude lower than in the bulk water.

Our predictions support the existing experimental data suggesting the following cell entry model for flecainide transport: (i) drug accumulates on the membrane surface in cationic and neutral forms; (ii) deprotonation occurs at the surface binding site (site 1) and promotes membrane crossing down the concentration gradient; and (c) drug acquires a proton once it is in the intracellular milieu.

As demonstrated in Fig. 4, virtual mouse and rabbit CASQ2(−/−) cells with β-agonist display increased Ca^{2+} transients and spontaneous Ca^{2+} release events, which are sufficient to drive triggered cellular electrical activity, and reproduce clinical behaviour of the CVPT phenotype (Liu *et al.* 2011*a*). The absence of calsequestrin as a buffer speeds up the dynamics of SR refilling, providing more interaction time for SR Ca^{2+} to activate the RyR2, and results in functionally upregulated RyR2 activity. The resulting spontaneous Ca^{2+} release events and depolarizations of the membrane persist after cessation of pacing, owing to cyclic refilling of the SR, spontaneous release of Ca^{2+} into the cytoplasm via the RyR2, activation of I_{Na} by inward I_{NCX}, influx of Ca^{2+} via activation of I_{CaL} and reuptake of Ca^{2+} into the SR via SERCA. It is important to note that diastolic intervals in the rabbit are longer than in the mouse, and the model predicted that they could allow sufficient time to promote spontaneous diastolic release and triggered activity. Our model predicted that high dose flecainide prevents aberrant spontaneous Ca^{2+} releases with resultant resolution of triggered AP activity in single virtual myocytes of mouse and rabbit and in rabbit transmural 1D virtual cardiac tissue (see Figs 6, 8 and 9), consistent with experimental data (Hilliard *et al.* 2010; Galimberti & Knollmann, 2011).

There is considerable disagreement in the literature as to whether the antiarrhythmic effects seen with flecainide are predominately the result of Na^+ channel blockade, RyR2 blockade, or both. Studies by Watanabe *et al.* (2009) and others (Hilliard *et al.* 2010; Galimberti & Knollmann, 2011; van der Werf *et al.* 2011) have documented a substantial interaction between flecainide and RyR2. They proposed that flecainide acts as a RyR2 open state blocker, with resultant increase in Ca^{2+} spark rate, a decrease in Ca^{2+} spark mass and disruption of Ca^{2+} wave propagation.

Other studies have failed to document any effects of flecainide on RyR or Ca^{2+} handling, and suggested flecainide's efficacy is almost entirely due to its Na^+ channel blocking effects (Liu *et al.* 2011*a*; Bannister *et al.* 2015). There are a few potential explanations for these disparate findings, including a lower than expected flecainide concentration within the cell in Liu's study, given rapid diffusion of neutral flecainide through the membrane and repartitioning within the bath solution, and potential mutation-induced lowered affinity of flecainide for RyR2.

When we decoupled flecainide's presumed RyR2 activity from its well-known Na^+ channel blockade, we were surprised to find that the model predicted that Na^+ channel blockade – even at the high clinical doses – was not sufficient to explain the antiarrhythmic effects seen clinically with flecainide. As seen in Fig. 6 and 8 (single cells) and Fig. 9 (1D tissue), pure Na^+ channel

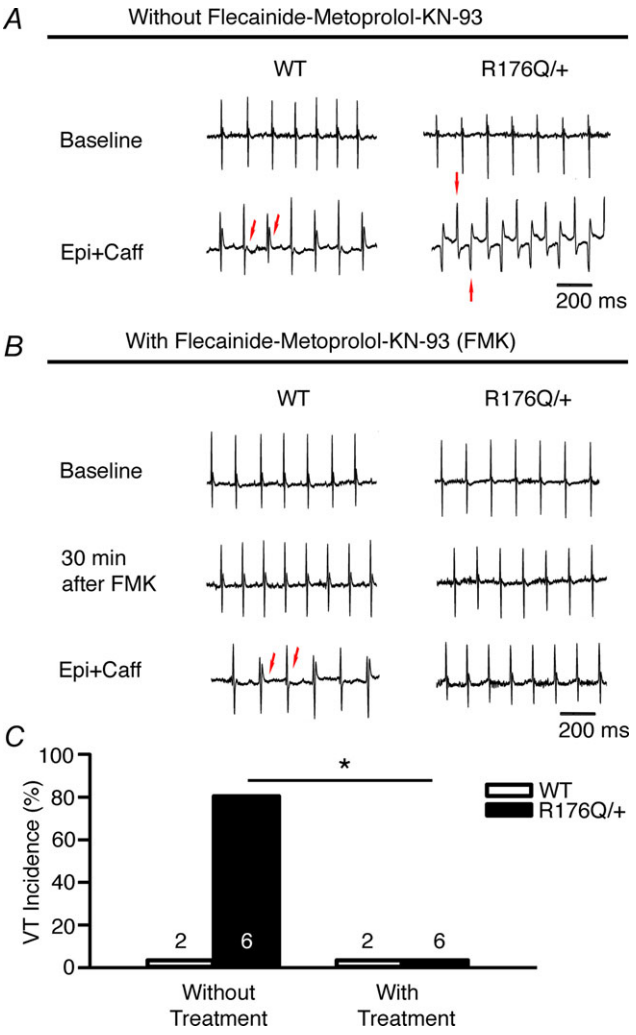

Figure 14. Experimental test of predicted polytherapy
A and *B*, representative tracings from WT and R176Q/+ mice are shown at baseline and after sympathetic challenge with no drug (*A*) and following administration of flecainide, metoprolol and KN-93 (*B*). *C*, summary of data without (left) and following (right) pre-treatment with flecainide, metoprolol and KN-93, which suppressed VT in all R176Q/+ mice (*$P = 0.015$).

Table 7. ECG measurement comparing wild type and R176Q/+ mice before and after treatments

	Without treatment						With treatment								
	Baseline			Epi + Caffeine			Baseline			Flec + Metop + KN-93			Epi + Caffeine		
	WT	R176Q/+	*P*	WT	R176Q/+	*P*	WT	R176/+	*P*	WT	R176Q/+	*P*	WT	R176Q/+	*P*
Heart rate (beats min^{-1})	574	462	0.18	588	466	0.09	442	467	0.73	385	375	0.93	424	328	0.25
PR (ms)	35	38	0.34	36	40	0.26	36	38	0.40	45	50	0.60	43	55	0.23
QRS (ms)	12	11	0.72	13	15	0.08	12	12	0.78	16	16	0.76	18	21	0.63
QTc (ms)	45	46	0.69	46	49	0.28	49	49	0.99	45	48	0.26	45	43	0.37

Adrenaline (2 mg kg^{-1}) and caffeine (120 mg kg^{-1}) were initially injected intraperitoneal (i.p.) without pre-treatment (Without treatment). Mice were then given a pre-treatment dose of flecainide (12 mg kg^{-1}, i.p.), metoprolol (10 mg kg^{-1}, i.p.), and KN-93 (30 μmol kg^{-1}, i.p.) followed 30 min later by an injection of the same i.p. dose of adrenaline and caffeine (With treatment). Flec, flecainide (12 mg kg^{-1}); Metop, metoprolol (10 mg kg^{-1}); KN-93 (30 μmol kg^{-1}).

blockade failed to inhibit spontaneous Ca^{2+} release, and subsequent triggered activity, whereas the RyR2-specific flecainide interaction was predicted to yield results similar to flecainide acting on both targets.

Interestingly, our simulations with lidocaine (Moreno *et al.* 2011) as an additional control of pure Na^+ channel blockade resulted in good concordance with experimental results (Katz *et al.* 2010; Galimberti & Knollmann, 2011; Hwang *et al.* 2011), namely that as a monotherapeutic approach, Na^+ channel blockade is insufficient to resolve CPVT arrhythmia triggers. Consistent with experimental evidence in support of this mechanism of action, flecainide's interaction with the Na^+ channel did resolve arrhythmia triggers in higher dimensions, but proarrhythmic DADs persisted.

Lastly, because the drugs used to treat CPVT act on different targets, we hypothesized that their actions might prove synergistic when used as a combination therapy. We tested the full parameter space of clinically relevant combination therapy with β-blockade, flecainide and CaMKII inhibition (Fig. 12), and found that all three drugs achieved better efficacy when used in combination with either or both of the other drugs tested. The potential to achieve therapeutic efficacy at lower drug concentrations potentially limits the danger of off-target and drug-related side-effects and are consistent with clinical reports of improved therapy with combined β-blockade and flecainide (Pott *et al.* 2011; Pflaumer & Davis, 2012).

Importantly, our polypharmacy simulations go beyond confirmation that a multidrug regimen is superior; for the first time (to our knowledge), our simulations are a proof-of-concept for prediction of a dosing strategy, and simulate a virtual phase 1–2 clinical trial of dose escalations with several thousand combinations of clinically relevant dosages.

We then utilized an experimental protocol to validate the virtual trial in R176Q/+ CPVT mice (Fig. 14). The CPVT R176/+ mice developed bidirectional ventricular tachycardia (VT) with catecholamine provocation. But, as predicted by the computer model in both rabbit (Fig. 12) and mouse (Fig. 13) virtual myocytes, pre-treatment with flecainide, metoprolol and KN-93 prevented catecholaminergically induced ventricular tachycardia in all R176Q/+ mice.

Table 8. Comparison of ECG measurements before and after treatment with flecainide, metoprolol and KN-93

	Baseline	Flecainide, Metoprolol, KN-93	*P*
Heart rate (beats min^{-1})	461	378	0.14
PR (ms)	37	48	0.01
QRS (ms)	12	16	< 0.001
QTc (ms)	49	47	0.12

Our study is not without limitations. Most importantly, different CPVT mutations demonstrate differences in ultrastructure (Liu *et al.* 2013), protein expression (Song *et al.* 2007), RyR2 structural conformation and functionality (Cerrone *et al.* 2005; Goddard *et al.* 2008), and Ca^{2+} dynamics (Viatchenko-Karpinski *et al.* 2004; Terentyev *et al.* 2006). As flecainide and β-blockade have been used clinically, we know that the adverse effect profiles are concentration dependent. Little is known about the clinical consequences of CaMKII inhibition, and our predictions will obviously require careful testing and validation prior to clinical use.

Another important limitation of our study is that the models that we have utilized do not explicitly represent subcellular Ca^{2+} dynamics. For this reason, we are not able to simulate subcellular Ca^{2+} waves and the effects of the drugs on them. This will be an important subject of a future study. In addition, a full experimental

follow-up study to further test and hone the therapeutic efficacy of alternate polytherapy approaches needs to be conducted.

In conclusion, we utilized a computational modelling approach, informed by, and validated with experimental and clinical data, to make therapeutic predictions of drug mechanism and efficacy in the setting of CPVT. Our study sought to answer three fundamental questions of current pharmacotherapy for CPVT. (i) Is flecainide interaction with the Na^+ channel sufficient for therapy? (ii) Can we predict if other Na^+ channel blockers will be equally efficacious? (iii) Can a multi-targeted pharmacologic approach synergize to yield greater success than with individual therapeutics?

References

Abrahamsson B, Lucker P, Olofsson B, Regardh CG, Sandberg A, Wieselgren I & Bergstrand R (1990). The relationship between metoprolol plasma concentration and beta$_1$-blockade in healthy subjects: a study on conventional metoprolol and metoprolol CR/ZOK formulations. *J Clin Pharmacol* **30**, S46–54.

Bannister ML, Thomas NL, Sikkel MB, Mukherjee S, Maxwell C, MacLeod KT, George CH & Williams AJ (2015). The mechanism of flecainide action in CPVT does not involve a direct effect on RyR2. *Circ Res* **116**, 1324–1335.

Belardinelli L, Liu G, Smith-Maxwell C, Wang WQ, El-Bizri N, Hirakawa R, Karpinski S, Li CH, Hu L, Li XJ, Crumb W, Wu L, Koltun D, Zablocki J, Yao L, Dhalla AK, Rajamani S & Shryock JC (2013). A novel, potent, and selective inhibitor of cardiac late sodium current suppresses experimental arrhythmias. *J Pharmacol Exp Ther* **344**, 23–32.

Boggara MB & Krishnamoorti R (2010). Partitioning of nonsteroidal antiinflammatory drugs in lipid membranes: a molecular dynamics simulation study. *Biophys J* **98**, 586–595.

Brugada J, Boersma L, Kirchhof C & Allessie M (1990). [Anisotropy and reentrant ventricular tachycardia: experimental model in the isolated rabbit heart]. *Rev Esp Cardiol* **43**, 558–568.

Brunton LL, Chabner BA & Knollmann BC (2010). *Goodman and Gilman's The Pharmacological Basis of Therapeutics*. McGraw-Hill Professional, New York, USA.

Cerrone M, Colombi B, Santoro M, di Barletta MR, Scelsi M, Villani L, Napolitano C & Priori SG (2005). Bidirectional ventricular tachycardia and fibrillation elicited in a knock-in mouse model carrier of a mutation in the cardiac ryanodine receptor. *Circ Res* **96**, e77–82.

Chudin E, Goldhaber J, Garfinkel A, Weiss J & Kogan B (1999). Intracellular Ca^{2+} dynamics and the stability of ventricular tachycardia. *Biophys J* **77**, 2930–2941.

Colquhoun D, Dowsland KA, Beato M & Plested AJ (2004). How to impose microscopic reversibility in complex reaction mechanisms. *Biophys J* **86**, 3510–3518.

Colquhoun D & Hawkes AG (1981). On the stochastic properties of single ion channels. *Proc R Soc Lond B Biol Sci* **211**, 205–235.

Davies SP, Reddy H, Caivano M & Cohen P (2000). Specificity and mechanism of action of some commonly used protein kinase inhibitors. *Biochem J* **351**, 95–105.

Di Pasquale E, Lodola F, Miragoli M, Denegri M, Avelino-Cruz JE, Buonocore M, Nakahama H, Portararo P, Bloise R, Napolitano C, Condorelli G & Priori SG (2013). CaMKII inhibition rectifies arrhythmic phenotype in a patient-specific model of catecholaminergic polymorphic ventricular tachycardia. *Cell Death Dis* **4**, e843.

Echt DS, Liebson PR, Mitchell LB, Peters RW, Obias-Manno D, Barker AH, Arensberg D, Baker A, Friedman L, Greene HL, *et al.* (1991). Mortality and morbidity in patients receiving encainide, flecainide, or placebo. The Cardiac Arrhythmia Suppression Trial. *N Engl J Med* **324**, 781–788.

Fedida D & Giles WR (1991). Regional variations in action potentials and transient outward current in myocytes isolated from rabbit left ventricle. *J Physiol* **442**, 191–209.

Fedida D, Orth PM, Hesketh JC & Ezrin AM (2006). The role of late I and antiarrhythmic drugs in EAD formation and termination in Purkinje fibers. *J Cardiovasc Electrophysiol* **17 Suppl 1**, S71–S78.

Galimberti ES & Knollmann BC (2011). Efficacy and potency of class I antiarrhythmic drugs for suppression of Ca^{2+} waves in permeabilized myocytes lacking calsequestrin. *J Mol Cell Cardiol* **51**, 760–768.

Gillespie DT (1977). Exact stochastic simulation of coupled chemical reactions. *J Phys Chem* **81**, 2340–2361.

Glukhov AV, Fedorov VV, Lou Q, Ravikumar VK, Kalish PW, Schuessler RB, Moazami N & Efimov IR (2010). Transmural dispersion of repolarization in failing and nonfailing human ventricle. *Circ Res* **106**, 981–991.

Goddard CA, Ghais NS, Zhang Y, Williams AJ, Colledge WH, Grace AA & Huang CL (2008). Physiological consequences of the P2328S mutation in the ryanodine receptor (RyR2) gene in genetically modified murine hearts. *Acta Physiol (Oxf)* **194**, 123–140.

Gyorke S & Terentyev D (2008). Modulation of ryanodine receptor by luminal calcium and accessory proteins in health and cardiac disease. *Cardiovasc Res* **77**, 245–255.

Hilliard FA, Steele DS, Laver D, Yang Z, Le Marchand SJ, Chopra N, Piston DW, Huke S & Knollmann BC (2010). Flecainide inhibits arrhythmogenic Ca^{2+} waves by open state block of ryanodine receptor Ca^{2+} release channels and reduction of Ca^{2+} spark mass. *J Mol Cell Cardiol* **48**, 293–301.

Huang L & Roux B (2013). Automated force field parameterization for nonpolarizable and polarizable atomic models based on ab initio target data. *J Chem Theory Comput* **9**, 3543–3556.

Hwang HS, Hasdemir C, Laver D, Mehra D, Turhan K, Faggioni M, Yin H & Knollmann BC (2011). Inhibition of cardiac Ca^{2+} release channels (RyR2) determines efficacy of class I antiarrhythmic drugs in catecholaminergic polymorphic ventricular tachycardia. *Circ Arrhythm Electrophysiol* **4**, 128–135.

Katz G, Khoury A, Kurtzwald E, Hochhauser E, Porat E, Shainberg A, Seidman JG, Seidman CE, Lorber A, Eldar M & Arad M (2010). Optimizing catecholaminergic polymorphic ventricular tachycardia therapy in calsequestrin-mutant mice. *Heart Rhythm* **7**, 1676–1682.

Kaurstad G, Alves MN, Kemi OJ, Rolim N, Hoydal MA, Wisloff H, Stolen TO & Wisloff U (2012). Chronic CaMKII inhibition blunts the cardiac contractile response to exercise training. *Eur J Appl Physiol* **112**, 579–588.

Knollmann BC, Chopra N, Hlaing T, Akin B, Yang T, Ettensohn K, Knollmann BE, Horton KD, Weissman NJ, Holinstat I, Zhang W, Roden DM, Jones LR, Franzini-Armstrong C & Pfeifer K (2006). Casq2 deletion causes sarcoplasmic reticulum volume increase, premature Ca^{2+} release, and catecholaminergic polymorphic ventricular tachycardia. *J Clin Invest* **116**, 2510–2520.

Kornyeyev D, Petrosky AD, Zepeda B, Ferreiro M, Knollmann B & Escobar AL (2012). Calsequestrin 2 deletion shortens the refractoriness of Ca^{2+} release and reduces rate-dependent Ca^{2+}-alternans in intact mouse hearts. *J Mol Cell Cardiol* **52**, 21–31.

Ledoux J, Chartier D & Leblanc N (1999). Inhibitors of calmodulin-dependent protein kinase are nonspecific blockers of voltage-dependent K^+ channels in vascular myocytes. *J Pharmacol Exp Ther* **290**, 1165–1174.

Leenhardt A, Lucet V, Denjoy I, Grau F, Ngoc DD & Coumel P (1995). Catecholaminergic polymorphic ventricular tachycardia in children. A 7-year follow-up of 21 patients. *Circulation* **91**, 1512–1519.

Li L, Vorobyov I, MacKerell AD & Allen TW (2008). Is arginine charged in a membrane? *Biophys J* **94**, L11–L13.

Liu H, Atkins J & Kass RS (2003). Common molecular determinants of flecainide and lidocaine block of heart Na^+ channels: evidence from experiments with neutral and quaternary flecainide analogues. *J Gen Physiol* **121**, 199–214.

Liu N, Denegri M, Dun W, Boncompagni S, Lodola F, Protasi F, Napolitano C, Boyden PA & Priori SG (2013). Abnormal propagation of calcium waves and ultrastructural remodeling in recessive catecholaminergic polymorphic ventricular tachycardia. *Circ Res* **113**, 142–152.

Liu N, Denegri M, Ruan Y, Avelino-Cruz JE, Perissi A, Negri S, Napolitano C, Coetzee WA, Boyden PA & Priori SG (2011*a*). Short communication: flecainide exerts an antiarrhythmic effect in a mouse model of catecholaminergic polymorphic ventricular tachycardia by increasing the threshold for triggered activity. *Circ Res* **109**, 291–295.

Liu N, Napolitano C, Venetucci LA & Priori SG (2012). Flecainide and antiarrhythmic effects in a mouse model of catecholaminergic polymorphic ventricular tachycardia. *Trends Cardiovasc Med* **22**, 35–39.

Liu N, Ruan Y, Denegri M, Bachetti T, Li Y, Colombi B, Napolitano C, Coetzee WA & Priori SG (2011*b*). Calmodulin kinase II inhibition prevents arrhythmias in $RyR2^{R4496C+/-}$ mice with catecholaminergic polymorphic ventricular tachycardia. *J Mol Cell Cardiol* **50**, 214–222.

Liu N, Ruan Y & Priori SG (2008). Catecholaminergic polymorphic ventricular tachycardia. *Prog Cardiovasc Dis* **51**, 23–30.

Marx SO, Gaburjakova J, Gaburjakova M, Henrikson C, Ondrias K & Marks AR (2001). Coupled gating between cardiac calcium release channels (ryanodine receptors). *Circ Res* **88**, 1151–1158.

Mehra D, Imtiaz MS, van Helden DF, Knollmann BC & Laver DR (2014). Multiple modes of ryanodine receptor 2 inhibition by flecainide. *Mol Pharmacol* **86**, 696–706.

Miyake CY, Webster G, Czosek RJ, Kantoch MJ, Dubin AM, Avasarala K & Atallah J (2013). Efficacy of implantable cardioverter defibrillators in young patients with catecholaminergic polymorphic ventricular tachycardia: success depends on substrate. *Circ Arrhythm Electrophysiol* **6**, 579–587.

Moreno JD, Yang PC, Bankston JR, Grandi E, Bers DM, Kass RS & Clancy CE (2013). Ranolazine for congenital and acquired late INa-linked arrhythmias: in silico pharmacological screening. *Circ Res* **113**, e50–61.

Moreno JD, Zhu ZI, Yang PC, Bankston JR, Jeng MT, Kang C, Wang L, Bayer JD, Christini DJ, Trayanova NA, Ripplinger CM, Kass RS & Clancy CE (2011). A computational model to predict the effects of class I anti-arrhythmic drugs on ventricular rhythms. *Sci Transl Med* **3**, 98ra83.

Morotti S, Edwards AG, McCulloch AD, Bers DM & Grandi E (2014). A novel computational model of mouse myocyte electrophysiology to assess the synergy between Na^+ loading and CaMKII. *J Physiol* **592**, 1181–1197.

Myles RC, Bernus O, Burton FL, Cobbe SM & Smith GL (2010). Effect of activation sequence on transmural patterns of repolarization and action potential duration in rabbit ventricular myocardium. *Am J Physiol Heart Circ Physiol* **299**, H1812–1822.

Nagatomo T, January C & Makielski J (2000). Preferential block of late sodium current in the LQT3 ΔKPQ mutant by the class IC antiarrhythmic flecainide. *Mol Pharmacol* **57**, 101–107.

Nakamura H, Kurokawa J, Bai CX, Asada K, Xu J, Oren RV, Zhu ZI, Clancy CE, Isobe M & Furukawa T (2007). Progesterone regulates cardiac repolarization through a nongenomic pathway: an in vitro patch-clamp and computational modeling study. *Circulation* **116**, 2913–2922.

Parikh A, Mantravadi R, Kozhevnikov D, Roche MA, Ye Y, Owen LJ, Puglisi JL, Abramson JJ & Salama G (2012). Ranolazine stabilizes cardiac ryanodine receptors: A novel mechanism for the suppression of early afterdepolarization and torsades de pointes in long QT type 2. *Heart Rhythm* **9**, 953–960.

Pflaumer A & Davis AM (2012). Guidelines for the diagnosis and management of Catecholaminergic Polymorphic Ventricular Tachycardia. *Heart Lung Circ* **21**, 96–100.

Pott C, Dechering DG, Reinke F, Muszynski A, Zellerhoff S, Bittner A, Kobe J, Wasmer K, Schulze-Bahr E, Monnig G, Kotthoff S & Eckardt L (2011). Successful treatment of catecholaminergic polymorphic ventricular tachycardia with flecainide: a case report and review of the current literature. *Europace* **13**, 897–901.

Priori SG, Napolitano C, Memmi M, Colombi B, Drago F, Gasparini M, DeSimone L, Coltorti F, Bloise R, Keegan R, Cruz Filho FE, Vignati G, Benatar A & DeLogu A (2002). Clinical and molecular characterization of patients with catecholaminergic polymorphic ventricular tachycardia. *Circulation* **106**, 69–74.

Rajamani S, Shryock JC & Belardinelli L (2008). Rapid kinetic interactions of ranolazine with HERG K^+ current. *J Cardiovasc Pharmacol* **51**, 581–589.

Roux B (1995). The calculation of the potential of mean force using computer-simulations. *Comp Phys Comm* **91**, 275–282.

Saucerman JJ, Brunton LL, Michailova AP & McCulloch AD (2003). Modeling β-adrenergic control of cardiac myocyte contractility in silico. *J Biol Chem* **278**, 47997–48003.

Sears SF Jr, Todaro JF, Lewis TS, Sotile W & Conti JB (1999). Examining the psychosocial impact of implantable cardioverter defibrillators: a literature review. *Clin Cardiol* **22**, 481–489.

Shannon TR, Wang F, Puglisi J, Weber C & Bers DM (2004). A mathematical treatment of integrated Ca dynamics within the ventricular myocyte. *Biophys J* **87**, 3351–3371.

Sikkel MB, Collins TP, Rowlands C, Shah M, O'Gara P, Williams AJ, Harding SE, Lyon AR & MacLeod KT (2013). Triple mode of action of flecainide in catecholaminergic polymorphic ventricular tachycardia: reply. *Cardiovasc Res* **98**, 327–328.

Sitsapesan R, Montgomery RA, MacLeod KT & Williams AJ (1991). Sheep cardiac sarcoplasmic reticulum calcium-release channels: modification of conductance and gating by temperature. *J Physiol* **434**, 469–488.

Soltis AR & Saucerman JJ (2010). Synergy between CaMKII substrates and β-adrenergic signaling in regulation of cardiac myocyte Ca^{2+} handling. *Biophys J* **99**, 2038–2047.

Song L, Alcalai R, Arad M, Wolf CM, Toka O, Conner DA, Berul CI, Eldar M, Seidman CE & Seidman JG (2007). Calsequestrin 2 (CASQ2) mutations increase expression of calreticulin and ryanodine receptors, causing catecholaminergic polymorphic ventricular tachycardia. *J Clin Invest* **117**, 1814–1823.

Starmer CF, Lastra AA, Nesterenko VV & Grant AO (1991). Proarrhythmic response to sodium channel blockade. Theoretical model and numerical experiments. *Circulation* **84**, 1364–1377.

Terentyev D, Kubalova Z, Valle G, Nori A, Vedamoorthyrao S, Terentyeva R, Viatchenko-Karpinski S, Bers DM, Williams SC, Volpe P & Gyorke S (2008). Modulation of SR Ca release by luminal Ca and calsequestrin in cardiac myocytes: effects of CASQ2 mutations linked to sudden cardiac death. *Biophys J* **95**, 2037–2048.

Terentyev D, Nori A, Santoro M, Viatchenko-Karpinski S, Kubalova Z, Gyorke I, Terentyeva R, Vedamoorthyrao S, Blom NA, Valle G, Napolitano C, Williams SC, Volpe P, Priori SG & Gyorke S (2006). Abnormal interactions of calsequestrin with the ryanodine receptor calcium release channel complex linked to exercise-induced sudden cardiac death. *Circ Res* **98**, 1151–1158.

The Cardiac Arrhythmia Suppression Trial (CAST) Investigators (1989). Preliminary report: effect of encainide and flecainide on mortality in a randomized trial of arrhythmia suppression after myocardial infarction. *N Engl J Med* **321**, 406–412.

Tokumitsu H, Chijiwa T, Hagiwara M, Mizutani A, Terasawa M & Hidaka H (1990). KN-62, 1-[*N*,*O*-bis(5-isoquinoline-sulfonyl)-*N*-methyl-l-tyrosyl]-4-phenylpiperazi ne, a specific inhibitor of Ca^{2+}/calmodulin-dependent protein kinase II. *J Biol Chem* **265**, 4315–4320.

van der Werf C, Kannankeril PJ, Sacher F, Krahn AD, Viskin S, Leenhardt A, Shimizu W, Sumitomo N, Fish FA, Bhuiyan ZA, Willems AR, van der Veen MJ, Watanabe H, Laborderie J, Haissaguerre M, Knollmann BC & Wilde AA (2011). Flecainide therapy reduces exercise-induced ventricular arrhythmias in patients with catecholaminergic polymorphic ventricular tachycardia. *J Am Coll Cardiol* **57**, 2244–2254.

van Oort RJ, McCauley MD, Dixit SS, Pereira L, Yang Y, Respress JL, Wang Q, De Almeida AC, Skapura DG, Anderson ME, Bers DM & Wehrens XH (2010). Ryanodine receptor phosphorylation by calcium/calmodulin-dependent protein kinase II promotes life-threatening ventricular arrhythmias in mice with heart failure. *Circulation* **122**, 2669–2679.

Viatchenko-Karpinski S, Terentyev D, Gyorke I, Terentyeva R, Volpe P, Priori SG, Napolitano C, Nori A, Williams SC & Gyorke S (2004). Abnormal calcium signaling and sudden cardiac death associated with mutation of calsequestrin. *Circ Res* **94**, 471–477.

Watanabe H, Chopra N, Laver D, Hwang HS, Davies SS, Roach DE, Duff HJ, Roden DM, Wilde AA & Knollmann BC (2009). Flecainide prevents catecholaminergic polymorphic ventricular tachycardia in mice and humans. *Nat Med* **15**, 380–383.

Watanabe H, Steele DS & Knollmann BC (2011). Mechanism of antiarrhythmic effects of flecainide in catecholaminergic polymorphic ventricular tachycardia. *Circ Res* **109**, 712–713.

Wilde AA, Bhuiyan ZA, Crotti L, Facchini M, De Ferrari GM, Paul T, Ferrandi C, Koolbergen DR, Odero A & Schwartz PJ (2008). Left cardiac sympathetic denervation for catecholaminergic polymorphic ventricular tachycardia. *N Engl J Med* **358**, 2024–2029.

Yang JH & Saucerman JJ (2012). Phospholemman is a negative feed-forward regulator of Ca^{2+} in β-adrenergic signaling, accelerating β-adrenergic inotropy. *J Mol Cell Cardiol* **52**, 1048–1055.

Zhu Y, Kyle JW & Lee PJ (2006). Flecainide sensitivity of a Na channel long QT mutation shows an open-channel blocking mechanism for use-dependent block. *Am J Physiol Heart Circ Physiol* **291**, H29–37.

Additional information

Competing interests

C.E.C. has a research grant from Gilead Sciences, not involved in this study.

Author contributions

P.-C.Y. and J.D.M. designed and performed simulations, analysed data, and prepared the manuscript; S.B.V.-B., M.-T.J. and S.N. designed and performed simulations; C.Y.M. and X.H.T. designed and performed experiments, and drafted the manuscript; E.G. analysed data, and revised the manuscript; C.E.C. designed simulations and experiments, analysed data, coordinated and oversaw the project, and prepared the manuscript. All authors have approved the final version of the manuscript and agree to be accountable for all aspects of

the work. All persons designated as authors qualify for authorship, and all those who qualify for authorship are listed.

Funding

American Heart Association (GIAs (10GRNT3880050, 13GRNT14370019), Western States Affiliate), the National Institutes of Health NHLBI RO1-HL-085592, NHLBI R01-HL-085592-S1, R01 HL105242-05, 1U01HL126273-01A1 and Gilead Sciences (to C.E.C.). Canadian Institutes for Health Research (MOP-186232) and Heart and Stroke Foundation, Alberta (GIA) (to S.N.). NIH-NHLBI (HL089598, HL091947, HL117641, HL129570), the American Heart Association (13EIA14560061) to XHT.